

# UV to FIR catalogue of a galaxy sample in nearby clusters: SEDs and environmental trends

Jonathan D. Hernández-Fernández<sup>1</sup>, J. Iglesias-Páramo<sup>1,2</sup>, and J. M. Vílchez<sup>1</sup>

Received \_\_\_\_\_; accepted \_\_\_\_\_

---

<sup>1</sup>Instituto de Astrofísica de Andalucía, Glorieta de la Astronomía s/n, 18008 Granada;  
jonatan@iaa.es

<sup>2</sup>Centro Astronómico Hispano Alemán C/ Jess Durbn Remón, 2-2 04004 Almería

## ABSTRACT

In this paper, we present a sample of cluster galaxies devoted to study the environmental influence on the star-formation activity. This sample of galaxies inhabits in clusters showing a rich variety in their characteristics and have been observed by the SDSS-DR6 down to  $M_B \sim -18$  and by the GALEX AIS throughout sky regions corresponding to several megaparsecs. We assign the broad-band and emission-line fluxes from ultraviolet to far-infrared to each galaxy performing an accurate spectral energy distribution for spectral fitting analysis. The clusters follow the general X-ray luminosity vs. velocity dispersion trend of  $L_X \propto \sigma_c^{4.4}$ . The analysis of the distributions of galaxy density counting up to the 5th nearest neighbor  $\Sigma_5$  shows: (1) the virial regions and the cluster outskirts share a common range in the high density part of the distribution. This can be attributed to the presence of massive galaxy structures in the surroundings of virial regions (2) The virial regions of massive clusters ( $\sigma_c > 550 \text{ km s}^{-1}$ ) present a  $\Sigma_5$  distribution statistically distinguishable ( $\sim 96\%$ ) from the corresponding distribution of low-mass clusters ( $\sigma_c < 550 \text{ km s}^{-1}$ ). Both massive and low-mass clusters follow a similar density-radius trend, but the low-mass clusters avoid the high density extreme. We illustrate, with Abell 1185, the environmental trends of galaxy populations. Maps of sky projected galaxy density show how low-luminosity star-forming galaxies appear distributed along more spread structures than their giant counterparts, whereas low-luminosity passive galaxies avoid the low-density environment. Giant passive and star-forming galaxies share rather similar sky regions with passive galaxies exhibiting more concentrated distributions.

*Subject headings:* galaxy - galaxy cluster - environment - multi-wavelength - SED

## 1. Introduction

The clusters of galaxies are excellent laboratories to study the influence of the environment on galaxies. This influence is formed by environmental processes which are combinations of interactions of galaxies with other components of the Universe; galaxies, dark matter and plasma. The highest peaks of density in the spatial distribution of these components are in the cores of galaxy clusters. The galaxy population in the centers of clusters reaches up to volume densities of  $10^3$  bright galaxies per  $\text{Mpc}^3$  on spatial scales of  $\sim 1$  Mpc and those galaxies have relative velocities of several hundreds of  $\text{km s}^{-1}$  (Cox, A. N. 2000). The mass of dark matter haloes of clusters is several orders of magnitude greater than the sum of masses of the stellar component of galaxies with mass-to-light ratios that range from 100 to  $500 M_{\odot}/L_{\odot}$  (Cox, A. N. 2000) opposite the mass-to-light ratio for stellar component which cover the range 1-10  $M_{\odot}/L_{\odot}$  (Bell et al. 2003). The pressure of the intracluster medium (ICM), which with  $n_e \sim 10^{-3} \text{ cm}^{-3}$  and temperatures goes from  $10^7$  to  $10^8$  K is enough high to acts on the gas component of galaxies (Gunn & Gott 1972).

Each of the interactions of galaxies with these components (galaxies, ICM, dark matter halo) has a contribution in the different environmental processes. The interaction of galaxies with the ICM dominates the gas stripping processes, where the interstellar medium of galaxies is stripped via various mechanisms, including viscous and turbulent stripping (Toniazzo & Schindler 2001), thermal evaporation (Cowie & Songaila 1977) and ram pressure stripping (Quilis et al. 2000). The tidal interactions among galaxies dominates the galaxy mergers or strong galaxy-galaxy interactions (Mihos 2004) and the galaxy harassment (Moore et al. 1996, 1998, 1999). The environmental process known as *strangulation*, *starvation*, or *suffocation* is dominated by the tidal interaction with the dark matter halo of the cluster which removes the hot gas halo of the galaxy (Bekki et al. 2002). The environmental processes act on the stellar and gas/dust components of a galaxy

modifying its gas content, the star formation level, the structural and dynamical parameters, etc. In one side, the intensity of the environmental processes depend on galaxy properties like the stellar mass or the compactness of stellar component. Also, the environmental influence depends on the environmental conditions and/or the cluster properties as the density of cluster components (galaxies, ICM, dark matter halo), the velocity field of the cluster, etc. Specifically, there is a controversy about the dependence on global cluster properties (e.g.  $\sigma_c$ ) of the star formation activity of cluster galaxy population. Numerous works point out there is no such correlation (Smail et al. 1998; Andreon & Ettori 1999; Ellingson et al. 2001; Fairley et al. 2002; De Propris et al. 2004; Goto 2005; Wilman et al. 2005; Andreon et al. 2006) while other works claim the presence of a relation between the star formation activity and the global cluster properties (Martínez et al. 2002; Biviano et al. 1997; Zabludoff & Mulchaey 1998; Margoniner et al. 2001).

The cores of galaxy cluster are located around the peaks of densities of these components but the volume density of cluster components converges to the field value towards regions outside the virial regions in distances of some virial radii (Cox, A. N. 2000; Rines et al. 2003). So, the transition between the cluster centers and the surroundings samples a broad range in environmental properties. The environmental processes act on galaxies with different intensity depending on the galaxy (dynamical or stellar) mass or luminosity (see Boselli & Gavazzi 2006, for a review), but in the most of previous works the observed trends of galaxy properties are restricted to giant  $L \gtrsim L^*$  galaxies. The UV luminosity has revealed as a good proxy of the recent star formation rate because is a tracer of the more short-lived stars  $\tau < 10^8$  yr (Kennicutt 1998) and the UV-optical colors as an excellent classifier between passive evolving galaxies and star-forming galaxies (Chilingarian & Zolotukhin 2011). On the other hand, the optical and near-infrared spectral ranges sample stellar populations with ages which go from  $10^9$  to  $10^{10}$  years (Kennicutt 1998; Martin et al. 2005). This give us some important insights into the global star

formation history of a galaxy i.e. the stellar mass, the time-scale of the star formation history, etc.

Following the former considerations, we will design a sample of clusters nearby enough for their galaxies be observed around the classical luminosity limit between giant and dwarf galaxies  $M_B=-18$  by the DR6 of SDSS. We stress the cluster galaxy population must be observed by different surveys from UV to FIR in the central regions of each cluster and its surroundings up to several times the size of virial region. This cluster sample allow us to study the environmental behavior of different properties (current star formation, stellar mass, attenuation, etc) of a galaxy population with a broad luminosity range inhabits environments as different as the center of galaxy clusters or their surroundings.

The remainder of the paper is organized as follows. In section 2, we describe the design of the cluster sample. In section 3, we describe the compilation of broad-band and emission line fluxes for the galaxy sample of the cluster sample. In section 4, we show the compilation of fluxes for the galaxy sample, color-color distributions and an example of the SED of a galaxy from the sample. In section 5 we discussed three different items: the bolometric X-ray luminosity vs. cluster velocity dispersion  $L_X-\sigma_c$  relation, the local density  $\Sigma_5$  distribution of galaxy population split by their membership to virial regions of low-mass/massive clusters and as a hint for future work and the sky projected density of giant/low-luminosity and passive/star-forming galaxy population in a massive cluster. We summarized our findings in section 6

## 2. Cluster sample selection

One of the purpose of the sample design is embrace a luminosity range for the cluster galaxy sample as wide to contain the classical limit between giant and dwarf galaxies,

$M_B=-18$ . This constrains the redshift range of the cluster sample. The cluster sample is observed in a sky area which is delimited by the intersection of observed sky areas of SDSS and GALEX surveys. Both surveys are not completed (at the moment of sample definition, March 2008) and have smaller observed sky areas than the other ended surveys, 2MASS and IRAS. In order to sample a broad range of environments, we select galaxy clusters observed by these surveys up to regions several virial radius beyond the virial region. So, we discard those clusters with a poor sky coverage not only in the central regions but even in the outskirts of clusters.

In the following, we describe the process to build the cluster sample. In a first step, we take a compilation of Galaxy Clusters from NED <sup>1</sup>. Thanks to this approach, we take account all cluster selection criteria in the literature; visual inspection, image-smoothing techniques, X-ray extended sources detection, Red Sequence algorithm, surveys around cD galaxies, etc. This avoid any kind of bias in the cluster selection. We have selected all astrophysical objects with NED Object Type set to **GClstr**.

We constrain the redshift range to reach down the absolute magnitude limit of dwarf galaxies. The Main Galaxy Sample of SDSS reach up to  $r'_{MGS} \sim 17.77$  (Strauss et al. 2002), while the absolute magnitude limit for dwarf galaxy starts at  $M_B^{Dwarf} = -18$  (Binggeli et al. 1988; Mateo 1998), so:

$$\left\{ \begin{array}{l} R = r'_{MGS} - 0.1837(g - r) - 0.0971 \quad (\text{Lupton, R. 2005}) \\ M_R \equiv M_B^{Dwarf} - (B - R) \\ \mu \equiv R - M_R \\ \log z = 0.2\mu - 8.477 + \log h \quad (\text{Local Universe, i.e. } cz \approx HD = 100hD) \end{array} \right.$$

with  $B$ ,  $R$  apparent Johnson magnitudes;  $M_B$ ,  $M_R$  absolute Johnson magnitudes;  $\mu$

---

<sup>1</sup>NASA/IPAC Extragalactic Database, <http://nedwww.ipac.caltech.edu/>

distance modulus;  $H \equiv 100h$  with  $H$  the Hubble’s constant and  $z$  redshift. We assume  $h=0.7$  in this work. Assuming the  $(B-R)$  values observed by Mobasher et al. (2003) and the  $(g-r)$  values observed by Blanton et al. (2003) for red and blue galaxies, we obtain a upper limit in redshift of:

$$\begin{cases} \text{Blue galaxies: } (B - R) \approx 0.8, (g-r) \approx 0.2 \Rightarrow z \approx 0.044 \\ \text{Red galaxies: } (B - R) \approx 2.0, (g-r) \approx 1.0 \Rightarrow z \approx 0.071 \end{cases}$$

Then, we choose  $z=0.05$  as the upper limit in redshift as a compromise between red and blue galaxies and initially start with a cluster sample from  $z=0$  to  $z=0.05$ . This initial sample contains 1575 clusters.

We check by eye the distribution of the SDSS plates and the GALEX fields for this cluster sample over a sky region up to a projected radius of some Abell radius (Abell 1958) from the center of each cluster. After that, we set the lower limit in redshift for the cluster sample to  $z=0.02$  because this redshift limit is enough to cover the sky area of a typical galaxy cluster with only a few SDSS plates (1.5 deg radius) or GALEX fields (0.5 deg radius). In a second step, we crosscorrelated the coordinates of cluster centers reported by NED with the position of the SDSS plates and the GALEX fields, in order to know what the cluster centers are, at least, in one SDSS plate and one GALEX field. This gives a cluster sample of 373 galaxy cluster with redshift from 0.02 to 0.05. In order to get a good SDSS sky coverage of clusters, we check by eye the sky coverage of SDSS Main Galaxy Sample up to a projected radius of  $2.2 R_{Abell}$  from the cluster center. For a subsequent procedure, we need an spectroscopic galaxy sample covering an sky region with this specific radius or more extensive. We select only those clusters with a good SDSS sky coverage over an sky area with this size. This selection gives a sample of 230 clusters for  $0.02 < z < 0.05$ .

The clusters from different catalogs have different selection and detection criteria and we do not control whether there are spurious clusters in some of these catalogs. On the

one hand, we have to clean our cluster sample from non confident clusters and possible artifacts. On the other hand, we need a reliable measure of the cluster velocity dispersion,  $\sigma_c$  in order to characterize a cluster sample with a broad range in  $\sigma_c$ , from poor to rich clusters. We solve this two issues using the procedure proposed by Poggianti et al. (2006) in their Appendix C but assuming cluster center reported by NED instead of Bright Cluster Galaxy (BCG) as the center of galaxy cluster.

In the first step, we select the galaxies inside 2.2 Abell radii from the NED center and within a redshift range defined by  $\Delta z = \pm 0.015$  from the cluster redshift given by NED. From these galaxies, we estimate the cluster redshift  $z_c$  and the cluster redshift dispersion  $\sigma_z$  as the median and the median absolute deviation, respectively. If  $\sigma_z$  is higher than 0.0017 ( $\approx \sigma_c = 500 \text{ km s}^{-1}$  at  $z=0$ ), we set  $\sigma_z$  to this value. This step is useful to avoid too much contamination from surrounding galaxy structures. Then, we computed the radius  $r_{200}$  from  $z_c$  and  $\sigma_z$  using the following equation:

$$r_{200} = 1.73 \frac{\sigma_c}{1000 \text{ km s}^{-1}} \frac{1}{\sqrt{\Omega_\lambda + \Omega_0(1 + z_c)^3}} h^{-1} \text{ Mpc} \quad (1)$$

which is taken from Finn et al. (2005). First, we recomputed  $z_c$  and then  $\sigma_z$  from those galaxies within  $\pm 3\sigma_z$  from  $z_c$  and more nearby to cluster center than  $1.2 r_{200}$ . This process iterates until it reaches the convergence. After each iteration, every galaxy in the initial sample can reenter to the cluster sample whether it meets the constraints on redshift and position. If the process does not converge, we discard that cluster. The error of the final  $\sigma_c$  is computed using a bootstrap algorithm applies to the galaxy sample in the cluster.

In this procedure, there are clusters which reach the convergence and show a final  $z_c$  far away from NED cluster redshift or with  $\sigma_z \gg 1000 \text{ km s}^{-1}$ . After a visual check to radial velocity histograms of these structures, we conclude those galaxy structures are far from be real clusters. In order to discard those structures, we add two constrains to the



cluster sample:

$$|z_c - z_{NED}| \leq 0.0033$$

$$\sigma_z \leq 1300 \text{ km s}^{-1}$$

After applying the procedure from Poggianti et al. (2006) and including this constrain to the former sample, the resulting sample is composed by 86 clusters. At the end of this procedure we still impose a further condition related to the presence of clusters with more than one NED identifier: NED only classifies two clusters from different catalogues as being the same cluster if their angular separation is less than 2 arcmin (Marion Schmitz - NED team, private communication). Using this clue, we take the cluster name from the most ancient catalogue to identify those clusters with more than one NED identifier.

As a final step, we visually check the GALEX AIS coverage of each cluster up to some Abell radius. We end up with 16 clusters in the redshift range  $0.02 < z < 0.05$ . Their basic properties are listed in Table 1. Their appearance in the sky and their radial velocity distributions are shown in figures 1 and 2, respectively. Figure 3 are the color-composite images of the central regions of clusters retrieved from the SDSS Navigate Tool <http://skyserver.sdss.org/public/en/tools/chart/navi.asp>.

Table 1: Main properties of the cluster sample.

$ID_{NED}$	$\alpha(J2000)$	$\delta(J2000)$	$z_{med}$	$\sigma_c$	$r_{200}$	$n_{200}$	$n_{tot}$	$\theta_{tot}$	$\log(L_X)$
	deg	deg		km s <sup>-1</sup>	Mpc			deg	L <sub>☉</sub>
(1)	(2)	(3)	(4)	(5)	(6)	(7)	(8)	(9)	(10)
UGCl 141	138.499	30.2094	0.0228	501.8	1.21	48	413	4.159	42.12
WBL 245	149.120	20.5119	0.0255	86.7	0.20	2	88	3.720	...
UGCl 148 NED01	142.366	30.2139	0.0263	316.7	0.76	21	354	3.606	...
ABELL 2199	247.154	39.5244	0.0303	756.2	1.83	313	1104	3.125	44.85
WBL 213	139.283	20.0403	0.0290	537.1	1.29	62	548	3.266	≤41.9
WBL 514(*)	218.504	3.78111	0.0291	633.7	1.52	88	580	3.257	43.18
WBL 210	139.025	17.7242	0.0287	433.3	1.06	56	402	3.298	43.22
WBL 234	145.602	4.27111	0.0291	243.6	0.58	6	87	3.262	...
WBL 205	137.387	20.4464	0.0288	679.8	1.60	37	527	3.289	...
UGCl 393	244.500	35.1000	0.0314	637.9	1.52	121	529	3.016	43.60
UGCl 391	243.352	37.1575	0.0330	407.0	0.97	8	637	2.874	...
B2 1621+38:[MLO2002]	245.583	37.9611	0.0311	607.3	1.46	95	1053	3.046	43.19
UGCl 271	188.546	47.8911	0.0305	323.2	0.72	23	181	3.104	...
ABELL 1185	167.699	28.6783	0.0328	789.3	1.90	228	754	2.894	43.58
ABELL 1213	169.121	29.2603	0.0469	565.7	1.35	98	305	2.021	43.77
UGCl 123 NED01	127.322	30.4828	0.0499	849.0	2.00	113	260	1.900	44.32

The description of this table is in the following page.

Table 1: Main properties of the cluster sample.

(1) NED identifier, (2) and (3) Celestial coordinates of cluster center from NED webpage, (4) Cluster average redshift, (5) Cluster velocity dispersion, (6) Radius 200, (7) No. of galaxies inside virial region with SDSS redshift, (8) No. of galaxies associated to each cluster selected by criteria exposed in section 3.1, (9) Half size of sky square region retrieved for each cluster, computed assuming the Local Universe approximation  $cz=HD$ , the small-angle approximation  $D_P=D\times\theta[\text{rad}]$  and a projected radius  $R_P=7.1$  Mpc (10) Bolometric X-ray luminosity from Mahdavi & Geller (2001) except for WBL 213 (Mahdavi et al. 2000). (\*) The historical criterion is not applied. In the case of WBL 514, we have selected WBL 514 instead of MKW07 because this object is split in two clusters by a late reference (Struble & Rood 1991). The source of the data is specified. Otherwise, the data are results from this work. The cluster compilation was carry out from NED updated at March 28, 2008.

Taking a look to the sky distribution of clusters from the sample in the figure 1, it can be seen the wide variety of the cluster sample in cluster richness and spatial structure and in some cases, the presence of galaxy structures around the virial regions of clusters. The richness goes from the poor cluster WBL 245 or WBL 234 with only a few galaxies in their central regions to the massive cluster ABELL 2199, which is assembled in the supercluster ABELL 2197 - ABELL 2199 - B2 1621+38:[MLO2002] or the cluster ABELL 1185, with clear evidence of galaxy structures as filaments. There are apparently "isolated" clusters as UGCl 271 or UGCl 148 NED01 opposite the example of WBL 514 with a close "twin" cluster, WBL 518 (Beers et al. 1995).

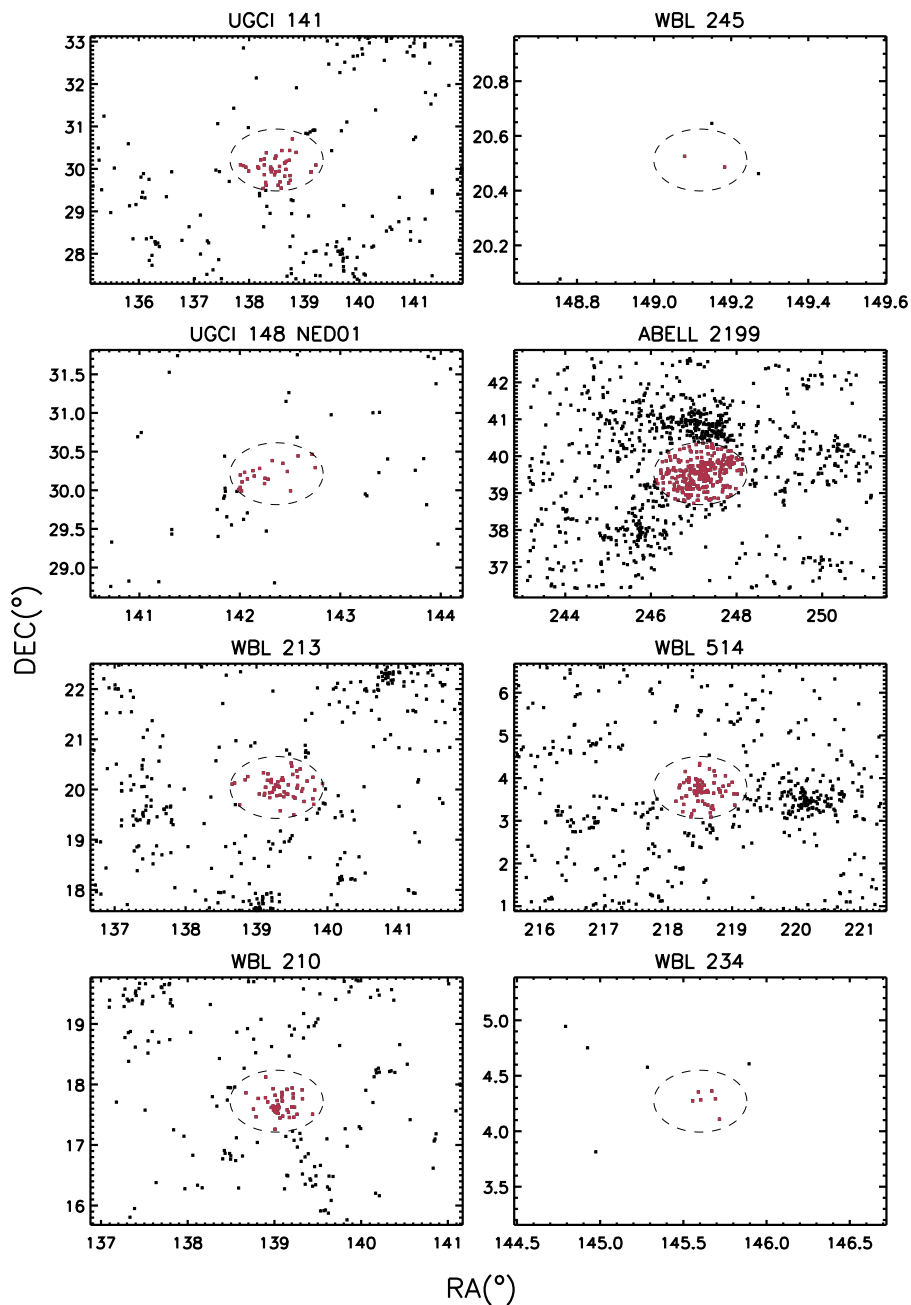


Fig. 1.— RA-DEC projection of the cluster sample. Ordinate axis is for declination and the abscissa axis is for right ascension. The red points correspond to galaxies in the virial region and the black points to the rest. All galaxies in the panels come from the DR6 of SDSS and are included in the cluster galaxy sample. In each panel, the dashed circle has a radius set to the  $r_{200}$  of each cluster. The size of each panel is set to  $8r_{200} \times 8r_{200}$ .

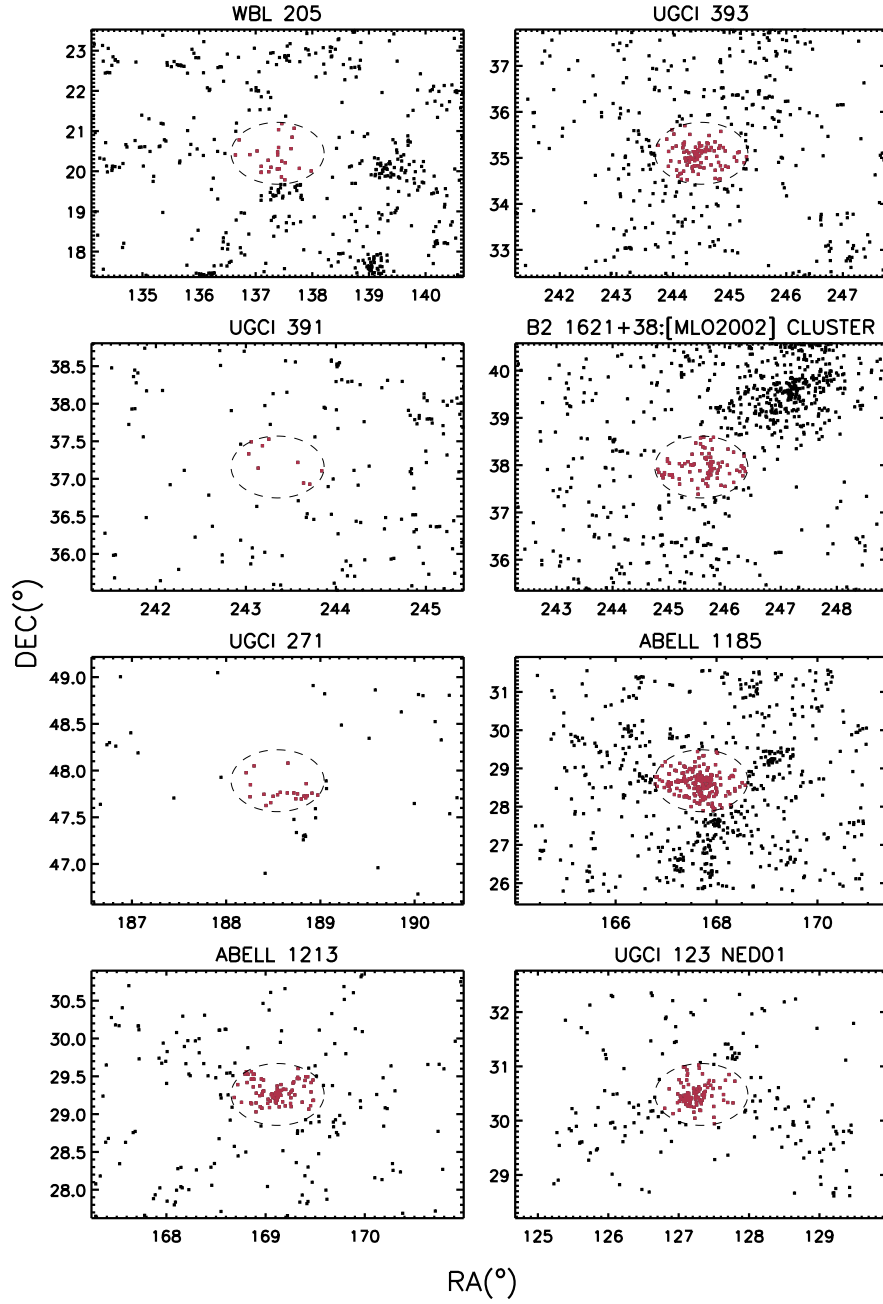


Fig. 1.— Continued.

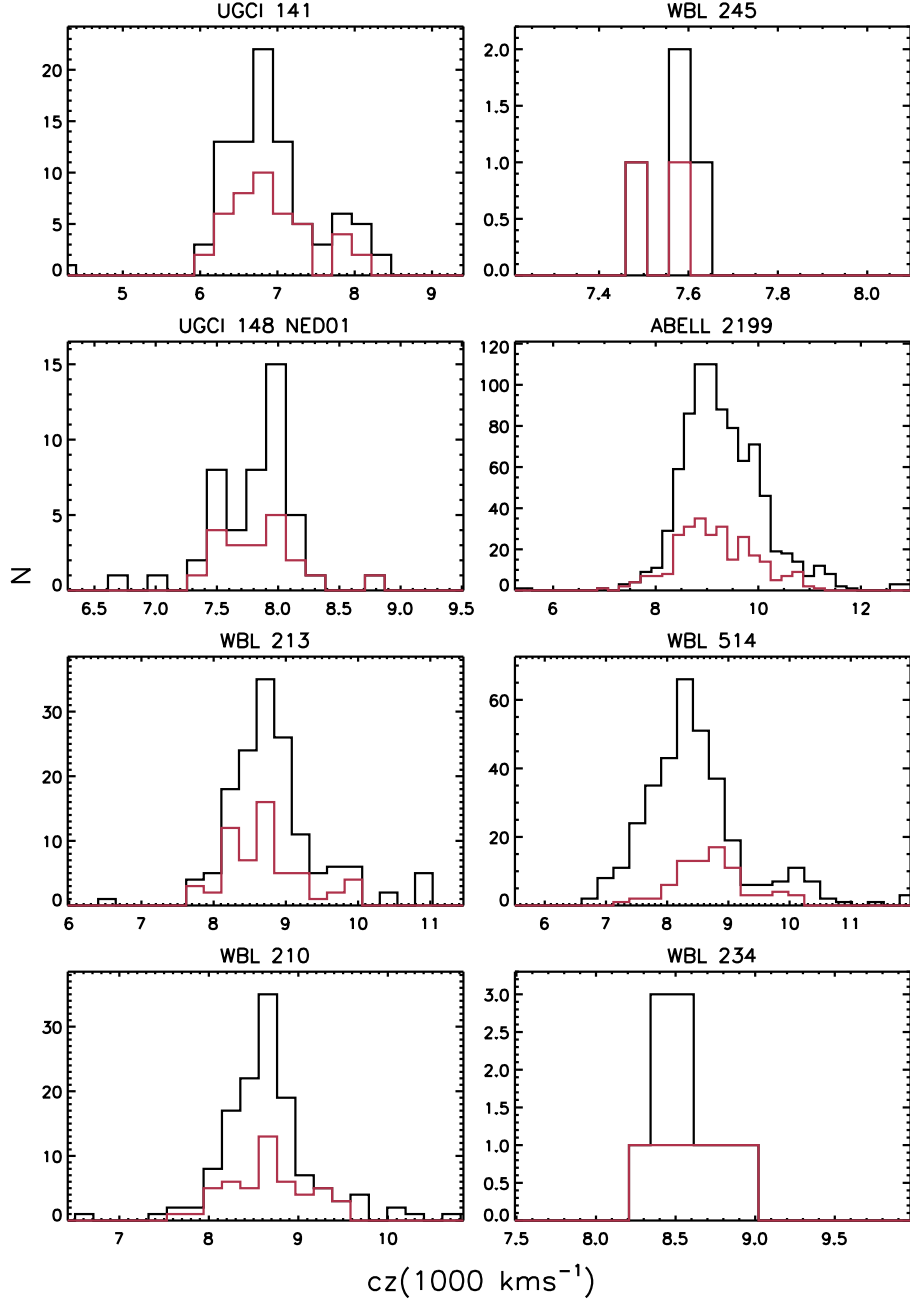


Fig. 2.— Radial velocity histograms for the cluster sample. The black histograms represent the galaxy sample inside a projected radius  $R_P$  three times the virial radius  $R_P < 3r_{200}$  and the red histograms correspond to those galaxies inside a projected radius set to one virial radius  $R_P < r_{200}$ . The range of abscissa in each panel is set to  $cz_c - 5\sigma_c < cz < cz_c + 5\sigma_c$  of each cluster.

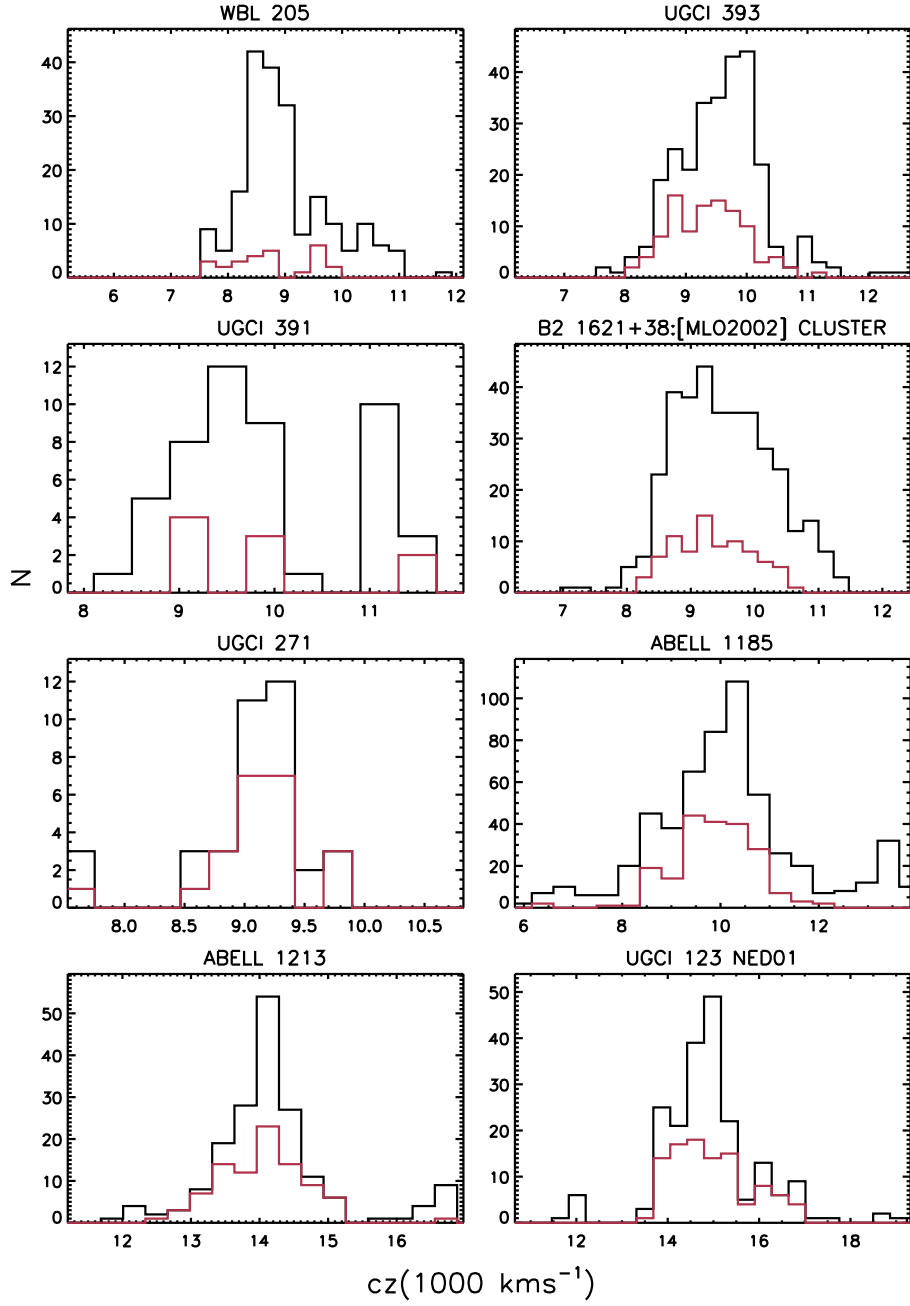


Fig. 2.— Continued.



### 3. Crossmatching of galaxy catalogues and compilation of spectrophotometric data

One purpose of this work is the compilation of broad-band and emission line fluxes from the ultraviolet around 1350 Å to the far-infrared around 100 μm for the cluster galaxy sample. In the last decades, this task becomes possible thanks to several sky surveys covering large areas of sky from UV to FIR. We present a brief summary about the main galaxy surveys from we retrieve spectrophotometric fluxes for the cluster galaxy sample and summarize the main figures of each survey in Table 2 :

- Galaxy Evolution Explorer (GALEX, Martin et al. 2005) was launched to, among others surveys, cover all sky at different depth and areas in two UV filters, the far-ultraviolet (*FUV*) band (1350-1750 Å) and the near-ultraviolet (*NUV*) band (1750-2750 Å). The AIS plans to survey the entire sky down to a sensitivity of  $m_{AB} \approx 20.5$ , comparable with the sensitivity of the SDSS Main Galaxy Sample,  $r'_{MGS} = 17.77$  (Strauss et al. 2002).
- The SDSS Project (6th Data Release in Adelman-McCarthy et al. 2008) retrieved spectra from, among other astronomical objects, all galaxies with  $r' < 17.77$  from the SDSS Imaging Catalog. The SDSS photometric system (Fukugita et al. 1996) cover from 3000 to 11000 Å in five broad band filters ( $u'$ ,  $g'$ ,  $r'$ ,  $i'$  and  $z'$ ).
- The Two Micron All Sky Survey (2MASS, Cutri et al. 2001) has uniformly scanned the majority of the sky in three near-infrared (NIR) bands, J (1.25 μm), H (1.65 μm), and K<sub>s</sub> (2.17 μm).
- The Infrared Astronomical Satellite (IRAS, Neugebauer et al. 1984) was a project to perform an unbiased, sensitive all sky survey at 12, 25, 60 and 100 μm, down to a limiting flux of 0.2 Jy at 60 μm. This mission produced two main catalogues; the

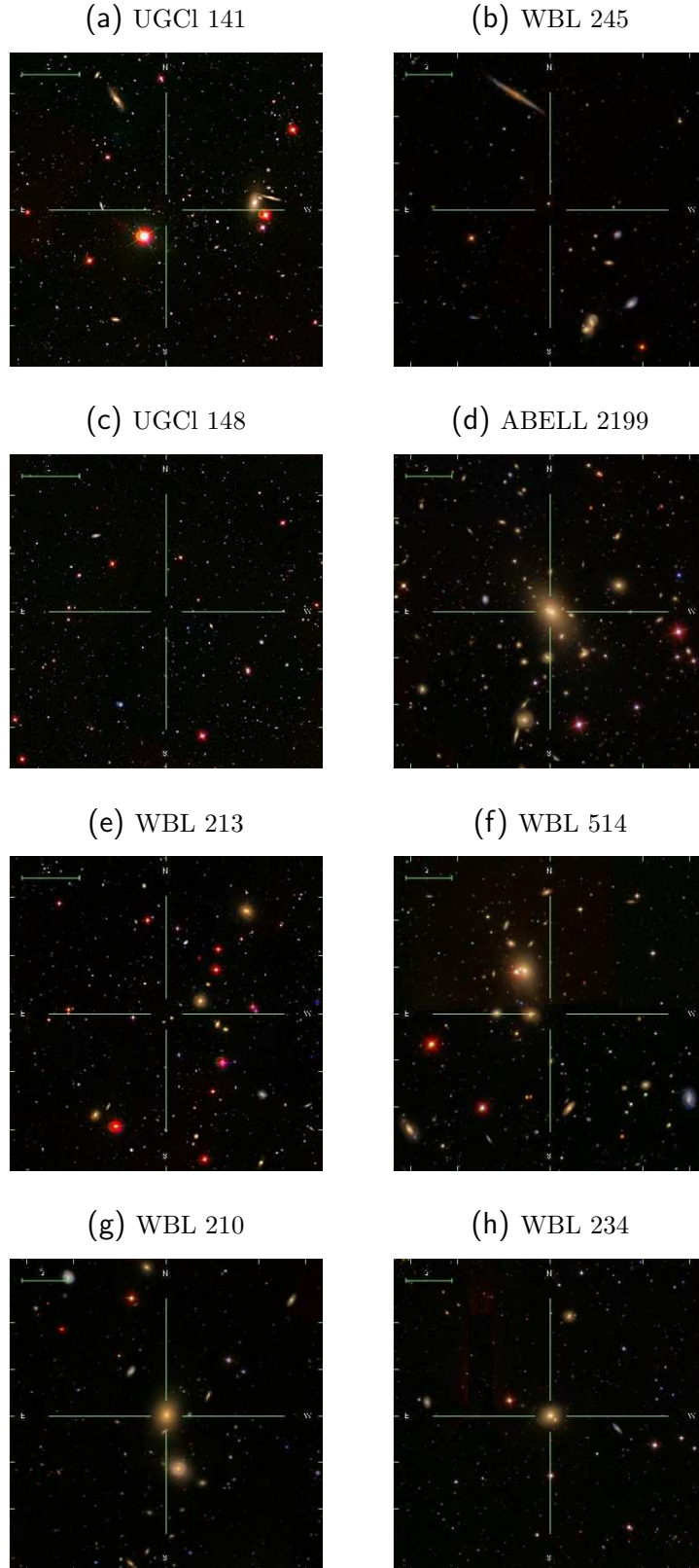


Fig. 3.— SDSS color-composite images of the central regions of clusters. The horizontal line in the upper left corner indicates the pixel-scale of the image.

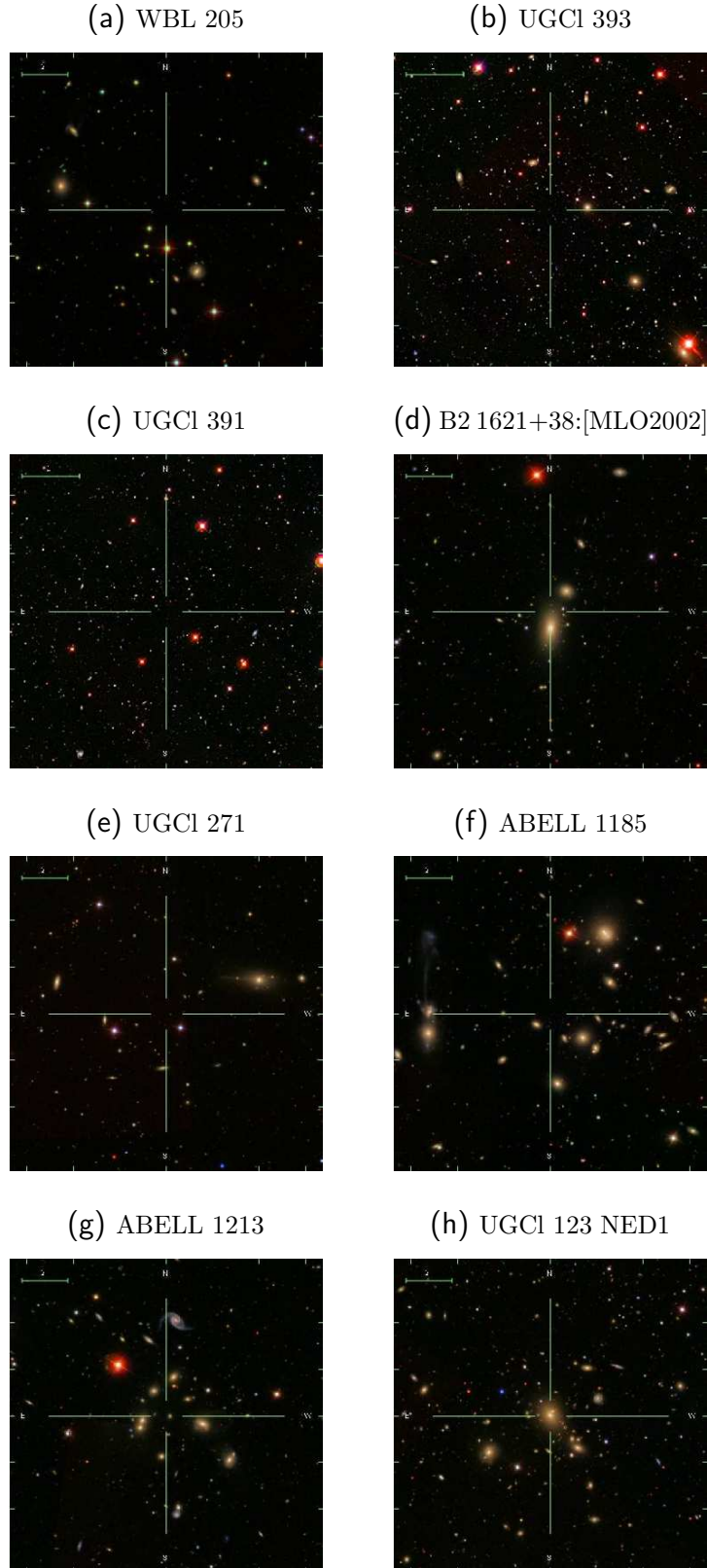


Fig. 3.— Continued.

Point Source Catalog catalogue (PSC, Joint Iras Science 1994) and the Faint Source Catalogue (FSC, Moshir et al. 1993).

### 3.1. SDSS data

The cross-correlation of celestial coordinates from different catalogues have been accomplished using the SDSS celestial coordinates as the fiducial coordinates. For each cluster, we retrieve all galaxies from the DR6 of SDSS with the following criteria:

- $R_P \leq 7.1$  Mpc
- $z_c - 5\sigma_c \leq z \leq z_c + 5\sigma_c$
- $z \geq 10^{-3}$  (In order to avoid stars in the lowest redshift clusters)

We retrieve photometric and spectroscopic data from SDSS database for this galaxy sample. The photometric fluxes come from the five broad-band filters of SDSS. We select the “*composite flux*” magnitude (Abazajian et al. 2004) as the suitable way to retrieve the total flux from each galaxy with the minimum uncertainty in color. We summed to the error reported by SDSS photometric pipeline (`photo`, Lupton et al. 2001) and the calibration errors reported in the DR6 of SDSS (Adelman-McCarthy et al. 2008), the standard deviation (based on the interquartile range) of distribution of the difference  $r_{composite} - r_{petrosian}$  to account uncertainties in color which are not present in the standard accurate-color photometry (i.e. petrosian magnitude, Abazajian et al. 2004).

We include spectroscopic data regarding to spectroscopic redshift and the fluxes for the four emission lines of the BPT diagram (Baldwin et al. 1981); [OIII] ( $\lambda=5007$  Å), H $\beta$  ( $\lambda=4861$  Å), [NII] ( $\lambda=6584$  Å) and H $\alpha$  ( $\lambda=6563$  Å). Moustakas et al. (2006) claim the

Table 2: Main figures of galaxy surveys.

SURVEY	band	$\lambda_c$	$\Delta\lambda_c$	$m_{lim}$
		$\mu\text{m}$	$\mu\text{m}$	AB mag
(1)	(2)	(3)	(4)	(5)
GALEX <sup>(a)</sup>	<i>FUV</i>	0.1550	0.400	20.5
	<i>NUV</i>	0.2250	1.000	20.5
SDSS <sup>(b)</sup>	<i>u'</i>	0.3551	0.599	22.0
	<i>g'</i>	0.4686	1.379	22.2
	<i>r'</i>	0.6165	1.382	22.2
	<i>i'</i>	0.7481	1.535	21.3
	<i>z'</i>	0.8931	1.370	20.5
2MASS <sup>(c)</sup>	<i>J</i>	1.25	1.620	16.39
	<i>H</i>	1.65	2.510	16.37
	<i>K<sub>s</sub></i>	2.17	2.620	16.34
IRAS(PSC+FSC) <sup>(d)</sup>	12 $\mu\text{m}$	12	7.00	10.64
	25 $\mu\text{m}$	25	11.15	10.64
	60 $\mu\text{m}$	60	32.5	10.64
	100 $\mu\text{m}$	100	32.5	8.9

(1) Survey, (2) Spectral band, (3) Central wavelength, (4) Spectral bandwidth and (5) Completeness limit. <sup>(a)</sup> Martin et al. (2005), <sup>(b)</sup> Adelman-McCarthy et al. (2008), <sup>(c)</sup> Finlator et al. (2000) and <sup>(d)</sup> Joint Iras Science (1994) + Moshir et al. (1993). Some galaxies in the FSC have upper limits with fluxes greater than these nominal values.

extinction-corrected  $H\alpha$  luminosity is a reliable Star Formation Rate (SFR) tracer, even in highly obscured star-forming galaxies. We derive galaxy SFRs from the extinction-corrected  $H\alpha$  luminosity. The extinction correction is applied using the Balmer decrement method and the Cardelli et al. (1989) extinction law with  $R_V=3.1$ . We take a HI recombination line ratio in the theoretical case B nebulae at  $T=10^4$  K as  $H\alpha/H\beta=2.87$ . We apply the scaling law between SFR and  $H\alpha$  luminosity proposed by Kennicutt (1998).

SDSS project has a pair of fiber-fed double spectrographs with 3 arcsec of fiber diameter on sky. This produces a loss of light from external parts of the largest galaxies. In order to reduce systematic and random errors from this “aperture effect” in SFR estimation Kewley et al. (2005) recommend selecting galaxy samples with the fiber capturing more than the 20% of the galaxy  $B_{445nm}$ -light. We assume a SDSS spectrum as representative of a galaxy when the fiber contains, at least, one fifth of the total  $g$ -band flux of the galaxy. So, we select these galaxies with:

$$(g_{fiber}-g_{model})\leq-2.5 \text{ alog}_{10}(0.2)$$

$g_{fiber}$  is the  $g$ -band magnitude measured inside an aperture similar to those produce by the SDSS fiber and  $g_{model}$  is the  $g$ -band “*model*” magnitude. In this case, we scale  $H\alpha$  fiber flux to  $H\alpha$  total flux using  $10^{-0.4(g_{model}-g_{fiber})}$  as scaling factor. Otherwise, we set  $H\alpha$  fiber flux (without any scaling) as the lower limit for the  $H\alpha$  total flux of these galaxies

### 3.2. SDSS-GALEX crosscorrelation

Following the criterium proposed by Obrić et al. (2006), we choose a matching radius of 6 arcsec between the SDSS and GALEX AIS celestial coordinates. We accomplish the

source matching using the GALEX application *GalaxView*<sup>2</sup>. In the case there is not a GALEX source in the matching circle, we do not assign an UV flux to SDSS source. The fraction of SDSS sources without GALEX detection is less than 20%. There are two options for the case of a non matched source; or this sky region is not observed by GALEX AIS, or the UV flux for the SDSS source is under GALEX AIS detection limit. The first case does not introduce a biased selection of galaxies i.e. there is no correlation between the celestial coordinates and the galaxy properties. In the second case, we have a completeness limit for the SDSS Main Galaxy Sample of  $r'_{MGS} < 17.77$  and the GALEX AIS reach down to  $NUV_{lim} \sim 22$  for Galactic extinction-corrected magnitudes, while the UV-optical color separation between blue and red galaxies is  $NUV-r \sim 4$ . So, this case only affects to red galaxies in the lowest flux bin  $r' \gtrsim 16$ .

We choose the elliptical aperture photometry (`MAG_AUTO` option in SExtractor code, Bertin & Arnouts 1996) for GALEX sources in order to have the complete UV flux for each source. These magnitudes are corrected from Galactic extinction using the excess color  $E(B-V)$  reported in GALEX tables for each UV source and assuming the Cardelli extinction law (Cardelli et al. 1989).

### 3.3. SDSS-2MASS crosscorrelation

The 2MASS project has enough image quality (FWHM  $\sim 2.5$ - $2.7$  arcsec, Cutri et al. 2001) to discriminate point-like sources (i.e. stars) from the extended ones (i.e. galaxies); the angular distance at  $z=0.05$  is  $0.977$  kpc arcsec<sup>-1</sup>. So, we only crosscorrelate the galaxy sample with the 2MASS All-Sky Extended Source Catalog (XSC) and not the 2MASS All-Sky Point Source Catalog (PSC). We follow Blanton et al. (2005) and set the matching

---

<sup>2</sup><http://galax.stsci.edu/GalaxView/#>

radius to 3 arcsec.

The NIR magnitudes for each SDSS source without 2MASS counterpart are fixed, as a lower limiting flux, to the completeness limit in each 2MASS band (Finlator et al. 2000). In this case, we set the error for the lower limit to a nominal value of  $\Delta m=1$  mag, which is the magnitude interval along the NIR galaxy counts decrease from the 100% completeness down to zero<sup>3</sup>. The matching rates vary from cluster to cluster and are around 40-60%.

We choose the photometry named *total magnitude* for the three NIR bands which is obtained from the integral between the lowest elliptical radius with a surface brightness of  $\mu=20$  mag arcsec<sup>-2</sup> (this corresponds to  $\sim 1\sigma$  of the sky background, Cutri et al. 2001) and a elliptical Srsic profile (Sérsic 1963) fitted to the surface brightness profile of the galaxy (Jarrett et al. 2000). We apply the magnitude conversion from Vega system to AB system from Finlator et al. (2000).

### 3.4. SDSS-IRAS crosscorrelation

Owing to the low angular resolution of IRAS telescope<sup>4</sup>, the galaxies resemble IRAS point-like sources. So, we crossmatch the galaxy sample with a joint catalogue of PSCz $\oplus$ FSC; *Point Source Catalogue* (Joint Iras Science 1994)  $\oplus$  *Faint Source Catalog* (Moshir et al. 1993). The FSC is  $\sim 2.5$  times deeper in limiting flux than the PSCz catalogue and the approximated flux frontier between this two catalogues is around 0.4 Jy. We set the matching radius to  $r=30$  arcsec, the value proposed by Blanton et al. (2005). Anyway, the matching rate is quite low  $\sim 1-5\%$ . The upper limit in IRAS flux for galaxies without IRAS counterpart is set to the values proposed for the FSC at each IRAS band

---

<sup>3</sup>[http://www.ipac.caltech.edu/2mass/releases/allsky/doc/sec2\\_3d3.html](http://www.ipac.caltech.edu/2mass/releases/allsky/doc/sec2_3d3.html)

<sup>4</sup><http://irsa.ipac.caltech.edu/IRASdocs/exp.sup/ch2/C3.html>



(Moshir et al. 1993). We set the upper limit error to the nominal (absolute+relative) error reported in PSCz catalogue:  $11\% + 0.06 \text{ Jy}$ .

#### 4. The spectrophotometric catalogue

The format of the spectrophotometric catalogue is presented in Table 3. It contains 53 columns that are described below, including the relevant observational parameters, spectrophotometric fluxes from UV to FIR and SFR estimates<sup>5</sup>:

Columns (1). ID: number associated to the position of the galaxy inside the cluster galaxy sample as a identifier.

Columns (2) and (3). ObjID and specObjID: SDSS Imaging Catalog and Main Galaxy Sample identifier of the galaxy.

Columns (4) and (5). RA and DEC: SDSS right ascension and declination (J2000) in degrees.

Columns (6) and (7).  $z$  and  $\epsilon_z$ : SDSS spectroscopic redshift and its uncertainty.

In sets of three elements, the following columns show the AB magnitude of galaxy, its uncertainty and the detection identifier<sup>(a)</sup> for the following spectral bands:

Columns ( 8), ( 9) and (10).  $AB_{FUV}$ ,  $\sigma_{FUV}$  and  $i_{FUV}$ : the GALEX  $FUV$  band.

Columns (11), (12) and (13).  $AB_{NUV}$ ,  $\sigma_{NUV}$  and  $i_{NUV}$ : the GALEX  $NUV$  band.

Columns (14), (15) and (16).  $AB_{u'}$ ,  $\sigma_{u'}$  and  $i_{u'}$ : the SDSS  $u'$  band.

Columns (17), (18) and (19).  $AB_{g'}$ ,  $\sigma_{g'}$  and  $i_{g'}$ : the SDSS  $g'$  band.

---

<sup>5</sup>The catalogue will be presented in its entirety in the online version of the paper.

Columns (20), (21) and (22).  $AB_{r'}$ ,  $\sigma_{r'}$  and  $i_{r'}$ : the SDSS  $r'$  band.

Columns (23), (24) and (25).  $AB_{i'}$ ,  $\sigma_{i'}$  and  $i_{i'}$ : the SDSS  $i'$  band.

Columns (26), (27) and (28).  $AB_{z'}$ ,  $\sigma_{z'}$  and  $i_{z'}$ : the SDSS  $z'$  band.

Columns (29), (30) and (31).  $AB_J$ ,  $\sigma_J$  and  $i_J$ : the SDSS  $J$  band.

Columns (32), (33) and (34).  $AB_H$ ,  $\sigma_H$  and  $i_H$ : the SDSS  $H$  band.

Columns (35), (36) and (37).  $AB_{K_s}$ ,  $\sigma_{K_s}$  and  $i_{K_s}$ : the SDSS  $K_s$  band.

Columns (38), (39) and (40).  $AB_{12\mu m}$ ,  $\sigma_{12\mu m}$  and  $i_{12\mu m}$ : the IRAS 12  $\mu m$  band.

Columns (41), (42) and (43).  $AB_{25\mu m}$ ,  $\sigma_{25\mu m}$  and  $i_{25\mu m}$ : the IRAS 25  $\mu m$  band.

Columns (44), (45) and (46).  $AB_{60\mu m}$ ,  $\sigma_{60\mu m}$  and  $i_{60\mu m}$ : the IRAS 60  $\mu m$  band.

Columns (47), (48) and (49).  $AB_{100\mu m}$ ,  $\sigma_{100\mu m}$  and  $i_{100\mu m}$ : the IRAS 100  $\mu m$  band.

Columns (50), (51) and (52). SFR,  $\sigma_{SFR}$  and  $i_{SFR}$ :  $H\alpha$ -derived star formation rate (SFR), its uncertainty and detection identifier in SFR.

Column (53). Cluster: identifier for the parent cluster of the galaxy. The cluster identifiers are codified in the following way: A=ABELL, B2=B2 1621+38:[MLO2002] CLUSTER, N=NED, U=UGCl, W=WBL.

<sup>(a)</sup> Code for detection identifiers:

**1**  $\equiv$  Source detected on this band,

**0**  $\equiv$  Source undetected on this band (upper limit in flux),

**-1**  $\equiv$  Source not observed on this band and

**-2**  $\equiv$  Lower limit in flux.

Table 3: Spectrophotometric catalogue of cluster galaxy sample.

ID	ObjID	specObjID	RA	DEC	$z$	$\epsilon_z$	$AB_{FUV}$	$\sigma_{FUV}$	$i_{FUV}$	$AB_{NUV}$	$\sigma_{NUV}$	$i_{NUV}$
(1)	(2)	(3)	(4)	(5)	(6)	(7)	(8)	(9)	(10)	(11)	(12)	(13)
			deg	deg			AB mag	AB mag		AB mag	AB mag	
1	587735239565377792	357982217034530816	134.655685	31.482407	0.02662	0.00009	19.049200	0.133216	1	18.683599	0.082258	1
2	587735240639381760	357982219328815104	134.670593	32.448460	0.02233	0.00009	-1.000000	1.000000	-1	-1.000000	1.000000	-1
3	587735043615096960	358263757475938304	135.079346	32.780834	0.02231	0.00009	-1.000000	1.000000	-1	-1.000000	1.000000	-1
4	587735043078946944	358263758667120640	136.960205	33.468132	0.02638	0.00017	21.178200	0.279031	1	19.302299	0.095046	1
5	587735239567474944	358545248592330752	139.522614	33.917965	0.02438	0.00016	-1.000000	1.000000	-1	21.215200	0.279032	1
6	587735239567540352	358545248617496576	139.730331	34.034649	0.02227	0.00018	-1.000000	1.000000	-1	21.621300	0.384734	1
7	587735239567540224	358545248625885184	139.611649	34.036049	0.02317	0.00020	-1.000000	1.000000	-1	21.976801	0.469288	1
8	587735239567737088	358545248667828224	140.089035	34.238449	0.02461	0.00008	-1.000000	1.000000	-1	18.375999	0.050605	1
9	587735239567605888	358545248823017472	139.744232	34.133747	0.02226	0.00015	-1.000000	1.000000	-1	-1.000000	1.000000	-1
10	587735042543124608	358545248831406080	139.641464	34.293934	0.02166	0.00014	-1.000000	1.000000	-1	20.270000	0.189778	1

NOTE: This table will be presented in its entirety in the online version of the paper.

Table 3: Continued.

ID	AB <sub>u'</sub>	$\sigma_{u'}$	i <sub>u'</sub>	AB <sub>g'</sub>	$\sigma_{g'}$	i <sub>g'</sub>	AB <sub>r'</sub>	$\sigma_{r'}$	i <sub>r'</sub>	AB <sub>i'</sub>	$\sigma_{i'}$	i <sub>i'</sub>	AB <sub>z'</sub>	$\sigma_{z'}$	i <sub>z'</sub>
(1)	(14)	(15)	(16)	(17)	(18)	(19)	(20)	(21)	(22)	(23)	(24)	(25)	(26)	(27)	(28)
	AB mag	AB mag		AB mag	AB mag		AB mag	AB mag		AB mag	AB mag		AB mag	AB mag	
1	18.517775	0.108053	1	17.700541	0.066168	1	17.592373	0.066663	1	17.379465	0.070090	1	17.194235	0.108876	1
2	19.067827	0.105126	1	18.039906	0.066950	1	17.741817	0.063210	1	17.584496	0.065851	1	17.514194	0.092795	1
3	19.101942	0.120221	1	17.946131	0.064513	1	17.827415	0.065841	1	17.913485	0.068607	1	17.935137	0.115220	1
4	16.447611	0.084428	1	14.826661	0.066261	1	14.076668	0.066026	1	13.676976	0.066025	1	13.416355	0.077062	1
5	17.861683	0.097150	1	16.316339	0.068362	1	15.610915	0.067196	1	15.253843	0.067416	1	15.014357	0.081505	1
6	19.127745	0.143379	1	17.663599	0.073838	1	16.970215	0.070757	1	16.692688	0.071775	1	16.589867	0.093554	1
7	19.035378	0.141855	1	17.719177	0.066303	1	17.065872	0.063679	1	16.616327	0.064424	1	16.577681	0.089601	1
8	17.831083	0.089150	1	16.744196	0.060600	1	16.188751	0.060178	1	16.101572	0.061675	1	16.413498	0.083945	1
9	18.705692	0.112631	1	17.124117	0.071256	1	16.368345	0.071518	1	16.046734	0.069902	1	15.803750	0.090045	1
10	16.759426	0.089591	1	15.192950	0.066689	1	14.493539	0.066356	1	14.086758	0.066258	1	13.676766	0.077599	1

Table 3: Continued.

ID	$AB_J$	$\sigma_J$	$i_J$	$AB_H$	$\sigma_H$	$i_H$	$AB_{K_s}$	$\sigma_{K_s}$	$i_{K_s}$	$AB_{12\mu m}$	$\sigma_{12\mu m}$	$i_{12\mu m}$
(1)	(29)	(30)	(31)	(32)	(33)	(34)	(35)	(36)	(37)	(38)	(39)	(40)
	AB mag	AB mag		AB mag	AB mag		AB mag	AB mag		AB mag	AB mag	
1	16.389999	0.500000	0	16.370001	0.500000	0	16.340000	0.500000	0	10.647425	0.410000	0
2	16.389999	0.500000	0	16.370001	0.500000	0	16.340000	0.500000	0	10.647425	0.410000	0
3	16.389999	0.500000	0	16.370001	0.500000	0	16.340000	0.500000	0	10.647425	0.410000	0
4	13.371000	0.024000	1	13.155000	0.036000	1	13.294000	0.041000	1	10.647425	0.410000	0
5	15.266000	0.056000	1	14.981000	0.064000	1	15.249000	0.089000	1	10.647425	0.410000	0
6	16.389999	0.500000	0	16.370001	0.500000	0	16.340000	0.500000	0	10.647425	0.410000	0
7	16.389999	0.500000	0	16.370001	0.500000	0	16.340000	0.500000	0	10.647425	0.410000	0
8	16.389999	0.500000	0	16.370001	0.500000	0	16.340000	0.500000	0	10.647425	0.410000	0
9	15.926000	0.086000	1	15.654000	0.107000	1	15.919000	0.156000	1	10.647425	0.410000	0
10	13.681000	0.026000	1	13.454000	0.035000	1	13.626000	0.051000	1	10.647425	0.410000	0

Table 3: Continued.

ID	AB <sub>25<math>\mu</math>m</sub>	$\sigma_{25\mu m}$	i <sub>25<math>\mu</math>m</sub>	AB <sub>60<math>\mu</math>m</sub>	$\sigma_{60\mu m}$	i <sub>60<math>\mu</math>m</sub>	AB <sub>100<math>\mu</math>m</sub>	$\sigma_{100\mu m}$	i <sub>100<math>\mu</math>m</sub>	SFR	$\sigma_{SFR}$	i <sub>SFR</sub>	Cluster
(1)	(41)	(42)	(43)	(44)	(45)	(46)	(47)	(48)	(49)	(50)	(51)	(52)	(53)
	AB mag	AB mag		AB mag	AB mag		AB mag	AB mag		$M_{\odot}\text{yr}^{-1}$	$M_{\odot}\text{yr}^{-1}$		
1	10.647425	0.410000	0	10.647425	0.410000	0	8.900000	0.170000	0	0.022868	0.012458	-2	U141
2	10.647425	0.410000	0	10.647425	0.410000	0	8.900000	0.170000	0	0.128186	0.052203	1	U141
3	10.647425	0.410000	0	10.647425	0.410000	0	8.900000	0.170000	0	0.208392	0.081589	1	U141
4	10.647425	0.410000	0	10.647425	0.410000	0	8.900000	0.170000	0	0.000000	0.590124	-2	U141
5	10.647425	0.410000	0	10.647425	0.410000	0	8.900000	0.170000	0	0.000000	0.074153	-2	U141
6	10.647425	0.410000	0	10.647425	0.410000	0	8.900000	0.170000	0	0.000000	0.007125	-2	U141
7	10.647425	0.410000	0	10.647425	0.410000	0	8.900000	0.170000	0	0.000000	0.003340	-2	U141
8	10.647425	0.410000	0	10.647425	0.410000	0	8.900000	0.170000	0	0.081989	0.027873	-2	U141
9	10.647425	0.410000	0	10.647425	0.410000	0	8.900000	0.170000	0	0.000000	0.021264	-2	U141
10	10.647425	0.410000	0	10.647425	0.410000	0	8.900000	0.170000	0	0.000000	0.183563	-2	U141

In Figure 4, we show the cluster galaxy sample in three UV-optical-NIR color-color diagrams; in each panel we show only galaxies with detection in the three corresponding spectral bands. Figure 4 shows how the galaxy sample traces the color distribution of the two main spectral types of galaxies; the passive galaxies and star-forming galaxies. The “red sequence” which is constituted by the family of passive galaxies becomes a “red clump” around  $(NUV-r)\sim 5.75$ ,  $(g-r)\sim 0.75$  and  $(r-K_s)\sim 1.0$  while the “blue cloud” of the star-forming galaxies turns into a sort of “blue sequence” which is more clearly visible in the UV-optical color diagram. We stress that the spectral information from UV bands allow us a more accurated selection of star-forming galaxies based on UV-optical color diagrams, cf. subsection 5.3 and figure 9. This is especially important for the study of a genuine sample of star-forming galaxies carried out in this and subsequent works.

The figure 5 shows an example of SED from the cluster galaxy sample composed by the broad-band fluxes and the SFR derived from  $H\alpha$  luminosity which covers three dex in wavelength and one dex in luminosity spectral density. The figure 5 highlights the importance of a consistent photometry capturing the total flux in each band along the SED in order to apply an accurate spectral fitting analysis. The figure 5 also illustrates the comparison of this SED with its best fitted spectral template from a synthetic spectral library in Hernández-Fernández (2011).

## 5. Discussion

In this work, we build up an extended catalogue of galaxies belonging to a sample of nearby clusters carefully selected to minimize cluster selection bias and to include a large diversity of cluster properties. Especial care has been exercised to follow a appropriate methodology producing a self consistent spectrophotometry along the SED. In this section we discuss the general properties of the selected clusters, together with the spectral

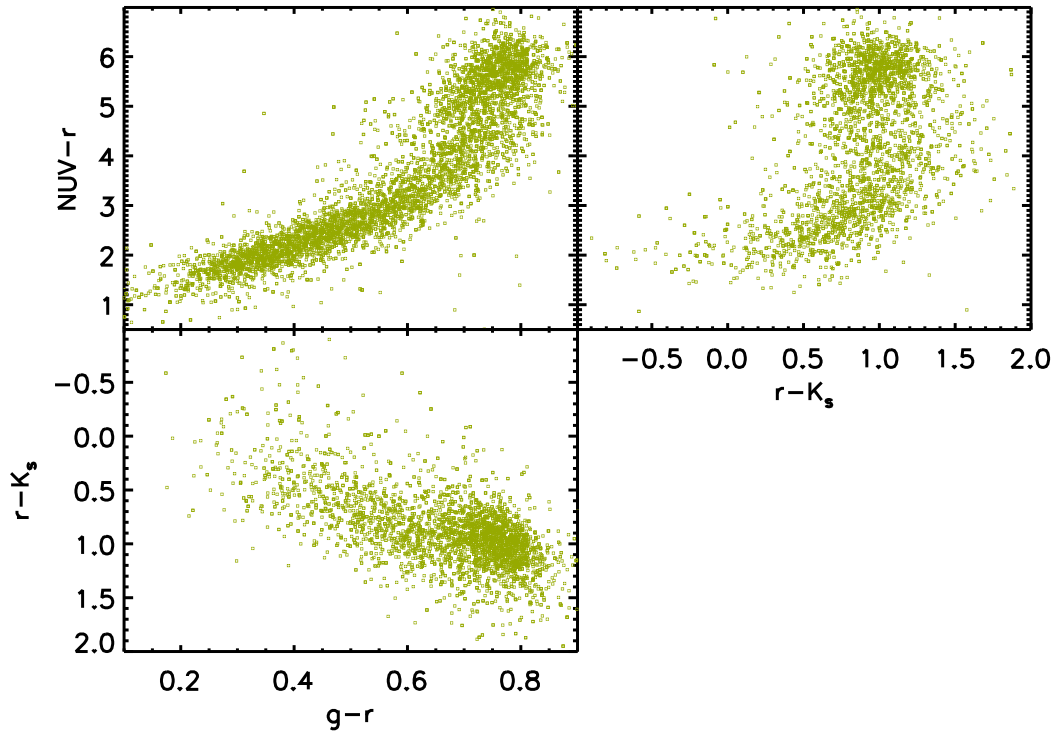


Fig. 4.— Color-color diagrams. From top to bottom, and from left to right:  $(NUV-r)$  vs.  $(g-r)$ ,  $(NUV-r)$  vs.  $(r-K_s)$  and  $(r-K_s)$  vs.  $(g-r)$  color-color diagrams.



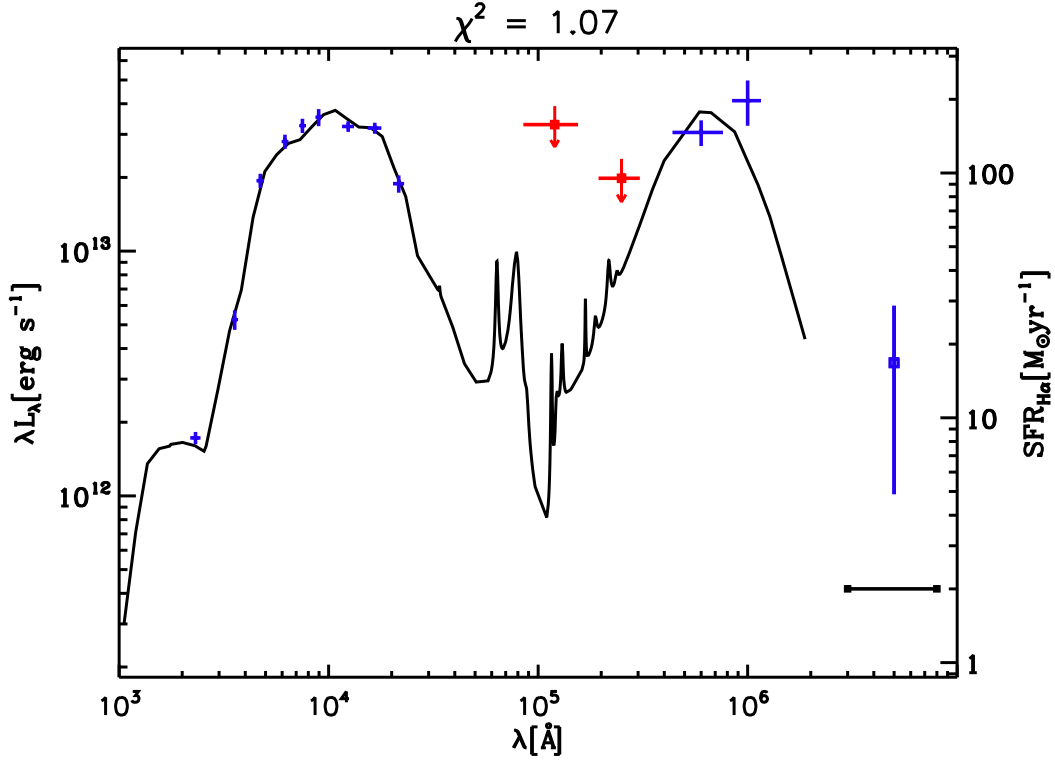


Fig. 5.— Example of a galaxy SED. The left ordinate axis presents the broad-band luminosity and the right ordinate axis the SFR. The solid line is the best fitted spectral template from a synthetic spectral library in Hernández-Fernández (2011). In the top of the graph, we show the value of chi-square for this fit. From left to right, blue data are the *NUV* band from GALEX, the five optical bands from SDSS, the three NIR bands from 2MASS, the 60 and 100  $\mu\text{m}$  IRAS bands and the  $\text{H}\alpha$ -SFR. Red data correspond to the upper limits in 12 and 25  $\mu\text{m}$  IRAS bands.

characterization of their galaxies and paying especial attention to the environmental trends of the sample.

### 5.1. X-ray luminosity vs. velocity dispersion

In figure 6, we plot bolometric X-ray luminosity vs. cluster velocity dispersion, the  $L_X\text{-}\sigma_c$  relation, for the cluster sample. The velocity dispersion and the associated errors are computed assuming the procedure proposed by Poggianti et al. (2006). The bolometric X-ray luminosity values are taken from Mahdavi et al. (2000) and Mahdavi & Geller (2001), assigning an uncertainty of 30% to the X-ray luminosity in the same way as Mahdavi & Geller (2001).

The  $L_X\text{-}\sigma_c$  relation for the galaxy clusters with associated X-ray detection (nine clusters) or an associated upper X-ray flux limit (WBL 213) follow in a consistent way the  $L_X\propto\sigma_c^{4.4}$  relation found by Mahdavi & Geller (2001) for a sample of 280 galaxy clusters. For some clusters of the sample, we did not find an associated X-ray source in Mahdavi & Geller (2001) catalogue neither one NED object with X-ray associated flux (**GGroups**, **GClusters** or **Xray** source) clearly associated to these clusters. Also, we know there is no sources with X-ray bolometric luminosities under  $10^{41}$  erg s<sup>-1</sup> in Mahdavi & Geller (2001) catalogue. Assuming these clusters are around or under this X-ray luminosity (with the typical uncertainties for these X-ray luminosities) this group would show a locus consistent with  $L_X\propto\sigma_c^{4.4}$  trend, except for the cluster WBL 205. In this cluster,  $\sigma_c$  is overestimated due to WBL 205 is clearly formed by two dynamical substructures (see figure 2).

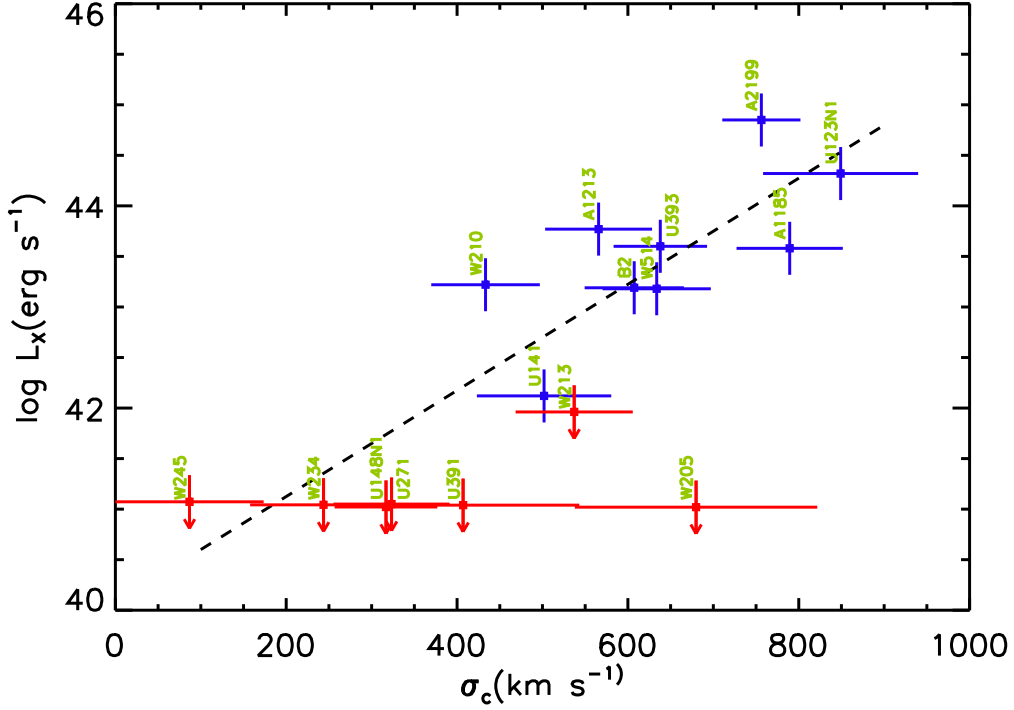


Fig. 6.—  $L_X$ - $\sigma_c$ . Bolometric X-ray luminosity vs. cluster velocity dispersion. Blue data points indicate X-ray detections and the red data point with  $L_X \sim 10^{42}$  erg s $^{-1}$  indicates a confident upper limit in X-ray luminosity. Red data points set to X-ray luminosities  $\sim 10^{41}$  erg s $^{-1}$  are associated to undetected X-ray sources. These data points are slightly displaced from  $L_X = 10^{41}$  erg s $^{-1}$  for the sake of clarity. The dashed line represent the  $L_X$ - $\sigma_c$  relation from Mahdavi & Geller (2001). The cluster identifier in the plot are codified in the following way: A=ABELL, B2=B2 1621+38:[MLO2002] CLUSTER, N=NED, U=UGCl, W=WBL.

## 5.2. Distribution and radial trend of the local galaxy density $\Sigma_5$

In Figure 7, we plot the distribution of local galaxy density of the cluster galaxy sample. We choose  $\Sigma_5$  as local density estimator following Balogh et al. (2004); this density is computed for each galaxy inside a circle containing up to the fifth neighboring galaxies more luminous than  $M_r=-20.6$  with radial velocities not farther than  $1000 \text{ km s}^{-1}$  from the radial velocity of each galaxy:

$$\Sigma_5 = \frac{5}{4\pi r_5^2} \quad (2)$$

with  $r_5$  the distance to the fifth neighboring galaxy more luminous than  $M_r=-20.6$  within  $\pm 1000 \text{ km s}^{-1}$  in radial velocity. We reject from  $\Sigma_5$  distributions galaxies with “edge effects”; those galaxies which some of their fifth first neighbors is placed far from the radial limits of galaxy sample (7 Mpc) or with a radial velocity out of the limits given by  $\pm 5\sigma_c$  around the cluster redshift. We consider four galaxy subsamples in two intervals of velocity dispersion of the parent cluster ( $\sigma_c < 550 \text{ km s}^{-1}$  - low-mass clusters and  $\sigma_c > 550 \text{ km s}^{-1}$  - massive clusters) and segregated by their membership to virial regions. The threshold for the cluster velocity dispersion  $\sigma_c = 550 \text{ km s}^{-1}$  between the low-mass and the massive clusters approximately matches a gravitational mass of  $2 \cdot 10^{14} M_\odot$  (Cox, A. N. 2000), a similar value to the characteristic mass of the distribution of cluster mass (Henry & Arnaud 1991). Also, Poggianti et al. (2006) choose a similar value for  $\sigma_c$  as a boundary between two distinct cluster environments with regard to their star formation activity; the massive clusters (those with a high  $\sigma_c$ ) are extremely hostile environments for star formation activity. They found a different trend of the [OII] emission-line fraction with the  $\sigma_c$  in these two cluster environments. The membership to the virial regions is assigned to galaxies inside a projected radius of  $r_{200}$  of each cluster and under the general caustic profile in a phase diagram obtained by Rines et al. (2003) for a sample of clusters in the Local Universe.

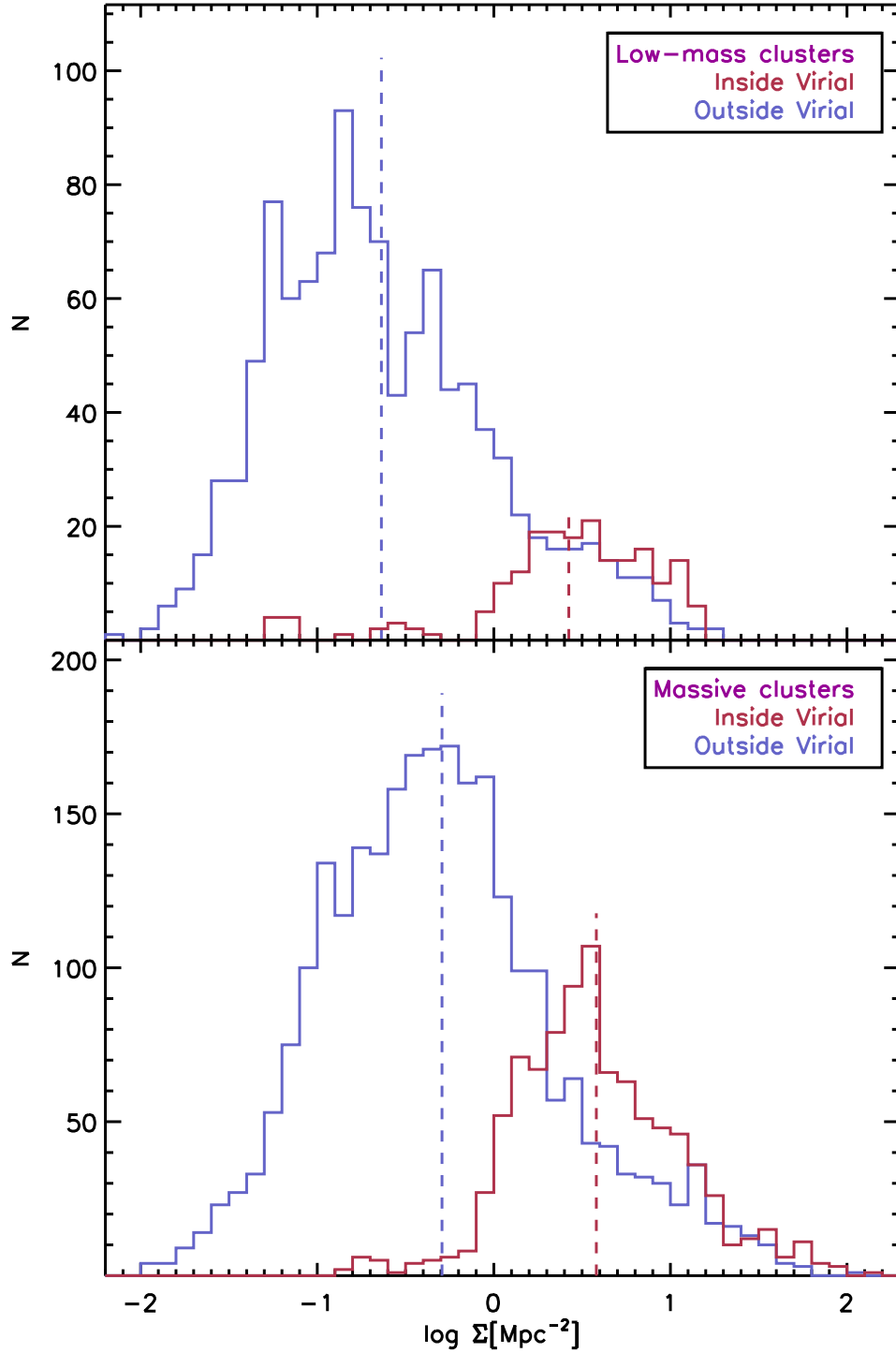


Fig. 7.—  $\Sigma_5$  distribution. Reddish/bluish histograms correspond to galaxies inside/outside virial regions. Top panel show low-mass clusters  $\Sigma_5$  distribution and the bottom panel, massive clusters  $\Sigma_5$  distribution. Vertical dashed lines show the mean value of  $\Sigma_5$  distribution in each case.

In a first look to figure 7, the  $\Sigma_5$  ranges from  $\sim 10^{-2}$  to  $\sim 10^2$ , a more broad range than the range of  $\Sigma_5$  distribution shown by Balogh et al. (2004) for two galaxy sample from SDSS DR1 (Sloan Digital Sky Survey Data Release I, Abazajian et al. 2003) and the  $\Sigma_5$  distribution of 2dFGRS (Two degrees Field Galaxy Redshift Survey, Colless et al. 2001) that go from  $\sim 3 \cdot 10^{-2}$  to  $\sim 30$ . In the higher density side, this difference comes from the lower statistics of this two samples ( $\sim 186240$  galaxies for SDSS DR1 and  $\sim 220000$  for 2dFGRS) versus the SDSS DR6 with  $\sim 790220$  galaxies i.e. this release contains a higher number of galaxies from the highest density regions, the clusters.

The  $\Sigma_5$  distribution of virial regions occupy the range  $-1 \lesssim \log \Sigma_5 \lesssim 1.2$  in both cases, massive clusters and low-mass clusters. Although, the high density tail of massive clusters ( $\log \Sigma_5 > 1.2$ ) is absent in the low-mass clusters. In addition, the mean of  $\Sigma_5$  for massive clusters ( $\log \Sigma_5 \approx 0.6$ ) is  $\approx 0.2$  dex higher than the mean of  $\Sigma_5$  for low-mass clusters. We apply a kolmogorov-Smirnov test to the  $\Sigma_5$  distributions of virial regions from the low-mass clusters and the massive clusters. They have a probability of  $\sim 4\%$  to come from the same parent population, so they are statistically distinguishable.

The  $\Sigma_5$  distribution of galaxies from the outskirts present a common range ( $-2 \lesssim \log \Sigma_5 \lesssim 1.3$ ). Further, two differences are noticed: (1) the presence of a high density tail ( $\log \Sigma_5 \gtrsim 1.3$ ) in massive clusters and (2) the mean of  $\Sigma_5$  in the outskirts of massive clusters ( $\log \Sigma_5 \approx -0.3$ ) is  $\approx 0.35$  dex higher than the corresponding mean for the low-mass clusters.

The difference between the mean of  $\Sigma_5$  for galaxies in virial regions and galaxies from the outskirts is more than one dex for the low-mass clusters versus the difference for massive clusters which is  $\approx 0.9$  dex. The overlapping in the high density side of  $\Sigma_5$  distributions between virial regions and the outskirts can be explained in the following way. The sample is designed following a set of observational constrains described in section 2 but the galaxy substructures around the virial region of selected clusters in the sample may not fulfill those

constrains. So, there may be galaxy structures in the outskirts of virial regions as massive as their parent cluster, the way one would expect from the similarity of the high density tails between virial regions and outskirts. Anyway, there is a  $\Sigma_5$  interval below  $\log\Sigma_5\sim 1$  where the galaxy subsample from the outskirts prevails over the galaxies from virial regions. Also, the absence of the highest density tail in the low-mass clusters is a clear evidence of the local density reach up their highest values in the more massive galaxy structures, the richest clusters.

In Figure 8, it can be seen a broad trend for the  $\Sigma_5-r_P$  relation ( $r_P\equiv R_P/r_{200}$ ), with the highest densities near to cluster centers at the top of a correlation in the virial region and the lowest densities far from the virial regions in the same way as found by Rines et al. (2005). We find the  $\Sigma_5-r_P$  relation is biased in  $\sim 0.5$  dex toward lower densities regarding the  $\Sigma_5-r_P$  relation obtained by Rines et al. (2005). This bias would come from a deeper luminosity cut for neighboring galaxies which is set to  $M_K=-22.7$ , enlarging the sample of neighboring galaxies devoted to compute the local density. The density-radius trend shows a more broad relation outside the virial region than the trend for the virial region. This came from the presence of galaxy structures which have peaks of density similar to those in the center of virial regions (e.g. ABELL 2197 or B2 1621+38:[MLO2002]). The massive clusters show galaxy structures with higher densities in the outskirts of virial regions than the low-mass clusters. Both the massive and low-mass clusters follow a similar trend inside the virial region, but the low-mass clusters reach only up to  $\log\Sigma_5\sim 1.2$  avoiding the highest density tail while the massive clusters reach up to  $\log\Sigma_5\sim 2$ . In the outskirts, the major concentration of galaxies in the lower side of the relation traces a common trend for both massive and low-mass clusters.

In Figure 8, we plot a King profile (King 1966) fit by eye to the major concentration of galaxy points along the  $\Sigma_5-r_p$  relation:

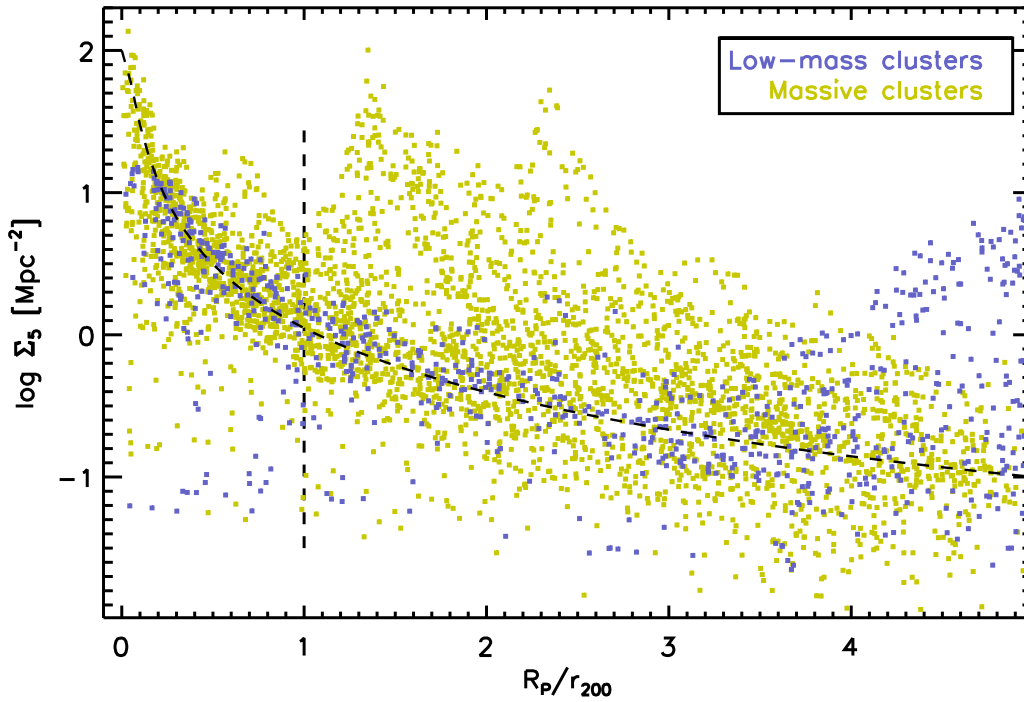


Fig. 8.—  $\Sigma_5$  vs.  $R_P/r_{200}$ . The projected density to fifth neighbor versus projected radius normalized to radius 200,  $r_P \equiv R_P/r_{200}$ . The legend identifies the subsample of clusters. The vertical dashed line delimit the a projected radius equal to  $r_{200}$ . The dashed curve is a King profile fit by eye to the main trend.



$$\log\Sigma = \log\Sigma^0 - \beta\log\left[1 + \left(\frac{r_p}{r_c}\right)^2\right], \quad \text{with } \Sigma^0 = 2, \beta = 0.75, r_c = 0.05 \quad (3)$$

The king profile was initially applied to the projected galaxy density of Coma cluster by King (1972). The fit from equation 3 in the  $\Sigma_5-r_p$  relation seems to reconcile the narrow relation inside the virial region with the concentration in the lower side of the relation for the surroundings. Both, the massive and low-mass clusters seem to follow the same relation along the clustercentric radius, with the massive clusters occupying the top of the density-radius fit.

### 5.3. Galaxy projected distribution

In this section we stress the relevance of a detailed mapping of the sky distribution of different galaxy populations as a tool for the study of environmental trends of galaxy properties. Such study is illustrated here for Abell 1185, a massive cluster of our sample. A similar analysis extended to the complete cluster sample is out of the scope of this paper and will be presented elsewhere (Hernández-Fernández et al. 2011b). We segregate galaxy populations according to their luminosity between giant galaxies  $M_r < -19.5$  and low-luminosity galaxies  $-19.5 < M_r < -18$ , and also to their spectral type between passive galaxies and star-forming galaxies. In order to differentiate passive galaxies from star-forming galaxies, we take advantage of the  $(NUV-r)$  vs.  $(u-r)$  color-color diagram. We assume a galaxy is a passive galaxy whether its colors fulfill the following prescription:

$$\left\{ \begin{array}{ll} NUV-r > 4.9 & \text{for } u-r < 2.175 \\ NUV-r > -2(u-r) + 9.25 & \text{for } u-r > 2.175 \\ u-r > 2.22 & \text{whether there is no GALEX counterpart} \end{array} \right.$$

As can be seen in Figure 9, this selection seems more accurated to differentiate star-

forming galaxies from passive galaxies than the  $u-r$  color cut proposed by Strateva et al. (2001). The broken line trace the minimum in the density of data points of ( $NUV-r$ ) vs. ( $u-r$ ) diagram between the maximum of density regarding the "red sequence" and the more extended maximum tracing the "blue cloud". The left side of the frontier tries to include in the passive galaxy side the locus of evolved "E+A" galaxies in a UV-optical diagram (Kaviraj et al. 2007). In the case there is no UV data for a galaxy, we apply the Strateva's  $u-r$  cut.

In a forthcoming paper (Hernández-Fernández et al. 2011a), we take advantage of this UV-optical color frontier in order to make up a sample of star-forming galaxies in clusters. We analyze the spatial variation of distributions of spectral properties for this sample of star-forming galaxies. We find statistically significant differences, applying a Kolmogorov-Smirnov test, in those distributions throughout different environments i.e. virial regions, infall regions and field environment.

The figures 10 and 11 show the sky distribution in Abell 1185 of giant galaxies  $M_r < -19.5$  and low-luminosity galaxies  $-19.5 < M_r < -18$ , respectively. Both figures, also show the sky distribution of star-forming and passive galaxies.

In Figure 10, it can be seen the main concentration of giant galaxies from the virial region of ABELL 1185 around  $RA \sim 167.75$  deg  $DEC \sim 28.5$  framed by the dashed circle. In the same way, there are evident galaxy agglomerations around the virial region of ABELL 1185 with less structural entity than ABELL 1185, except for the group of galaxies in the south side around  $RA \sim 167.8$  deg  $DEC \sim 27.5$ . We check the redshift distribution of galaxies around this location and find an evident dynamical structure around  $z=0.034$ . This aggregate of galaxies, showing a strikingly high fraction of passive giant galaxies, can be linked with the "bare" massive-cluster cores identified by Poggianti et al. (2006). Poggianti et al. (2006) propose, as a hypothesis, that systems close to more massive

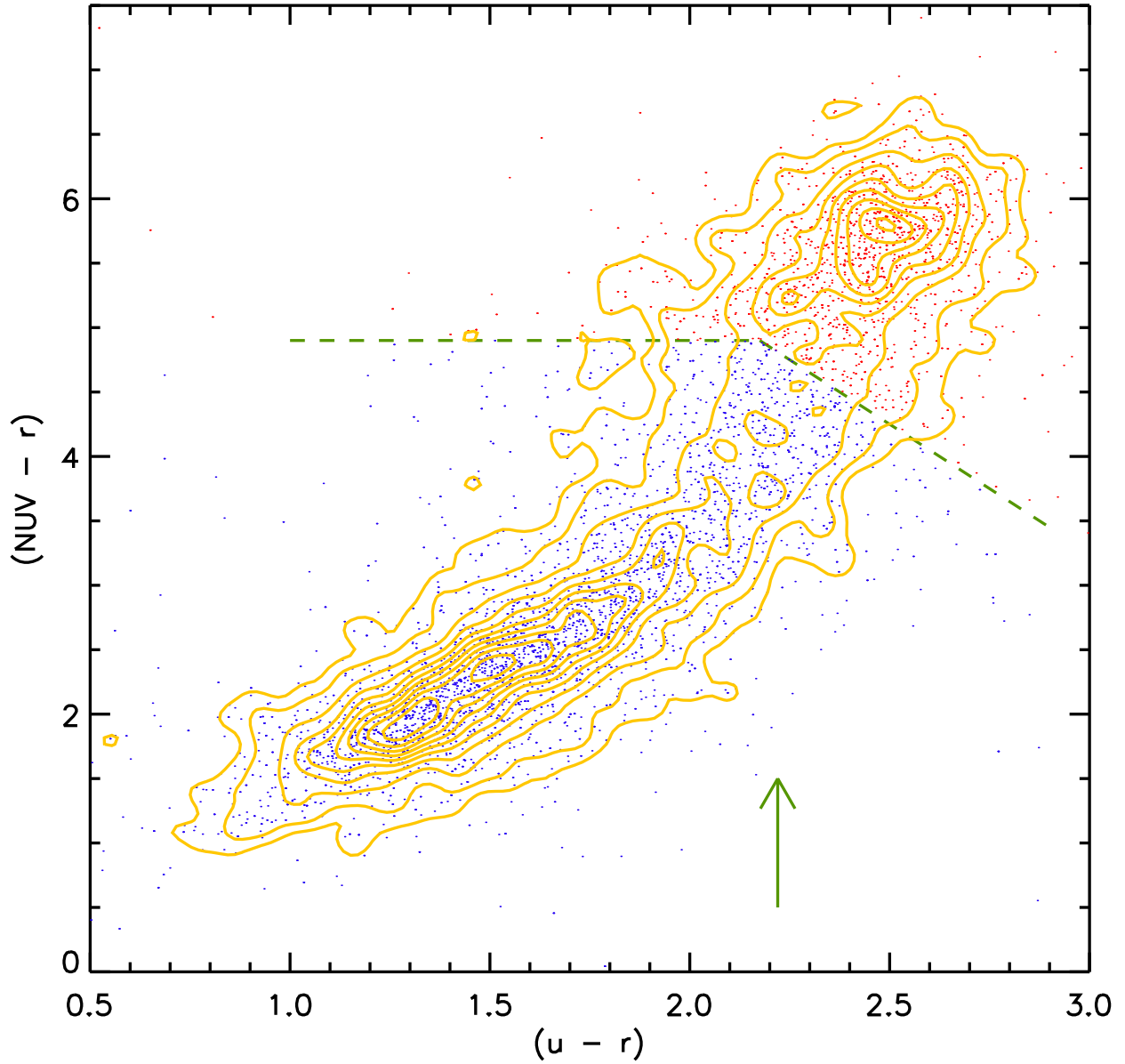


Fig. 9.—  $(NUV-r)$  vs.  $(u-r)$ . Yellow isocontours represents the isodensity contours of galaxies. Green dashed broken line is the color-color cut for galaxies with UV detection. Green vertical arrow points out to the  $u-r$  cut for galaxies without UV data. Blue and red points represent, respectively, star-forming and passive galaxies under the prescription shown in the section 5.3.

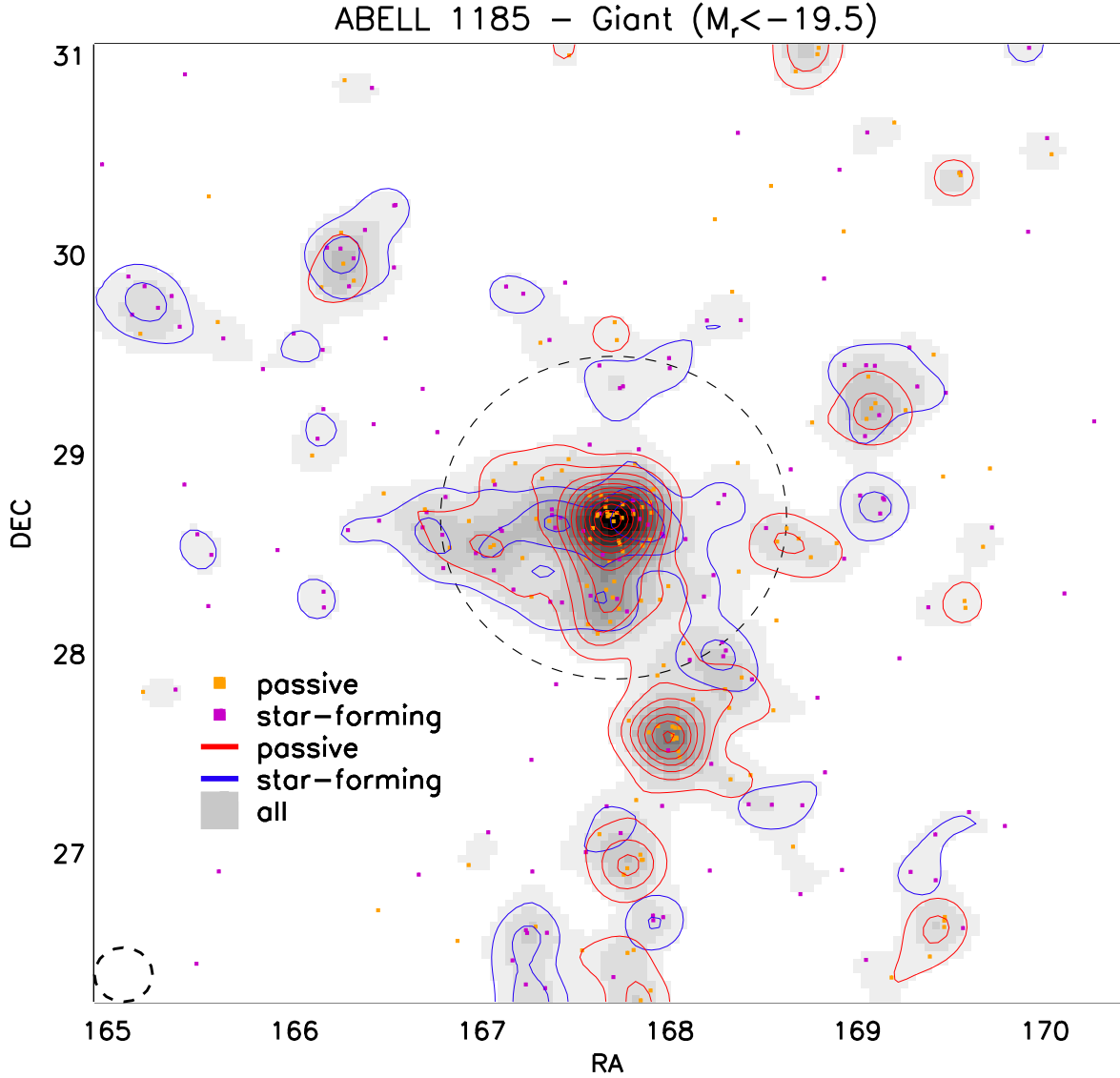


Fig. 10.— Sky projected density of giant  $M_r < -19.5$  galaxies around ABELL 1185. The grey intensity map corresponds to sky projected density of giant galaxies (both passive and star-forming galaxies). Orange/Magenta points represent sky position and red/blue contours represent isodensity lines of the sky projected density of giant galaxies classified as passive/star-forming galaxies. The lowest density contour correspond to a  $\Sigma=3$  gal/Mpc<sup>2</sup> and the contours are equispaced in  $\Delta\Sigma=3$  gal/Mpc<sup>2</sup> up to the maximum in density. The circle in the lower-left corner shows the FWHM size of gaussian kernel to compute the density map.

structures, thus embedded in a massive superstructure, have a different galactic content than completely isolated galaxy systems of similar mass. They suggest these objects lived in regions that were very dense at high redshift but failed to acquire star-forming galaxies at later times, possibly due to the characteristics of their surrounding supercluster environment. On the other hand, the maxima in the sky distribution of passive giant galaxies trace the central position of the main structures as ABELL 1185 and the “bare core” at the south side, while star-forming galaxies occupy these regions with a more spread distribution, following the general trend for clustering depending on spectral type founds in astrophysical observations and simulations (e.g., Madgwick et al. 2003; Springel et al. 2005).

We plot the sky distribution of low-luminosity  $-19.5 < M_r < -18$  galaxies in Figure 11. These galaxies show a more continuous sky distribution around the central region of ABELL 1185 connecting this region with the structures in the south, east and west side of the cluster. This is in good agreement with a less clustered low-luminosity population as suggested the literature (e.g., Norberg et al. 2002; Springel et al. 2005). The star-forming galaxies occupy both the densest regions and less dense regions, but the passive galaxies seem to inhabit preferably the central region of the structures avoiding the field environment in the same way as observed by Haines et al. (2006).

## 6. Summary

We expose the main results and conclusions of this paper in this itemized summary:

- We compile a sample of galaxies which inhabits in clusters showing a broad range of cluster properties ( $\sigma_c$ , morphology, etc). This galaxy sample is observed down to the luminosity frontier between giant and dwarf galaxies by the Main Galaxy Sample

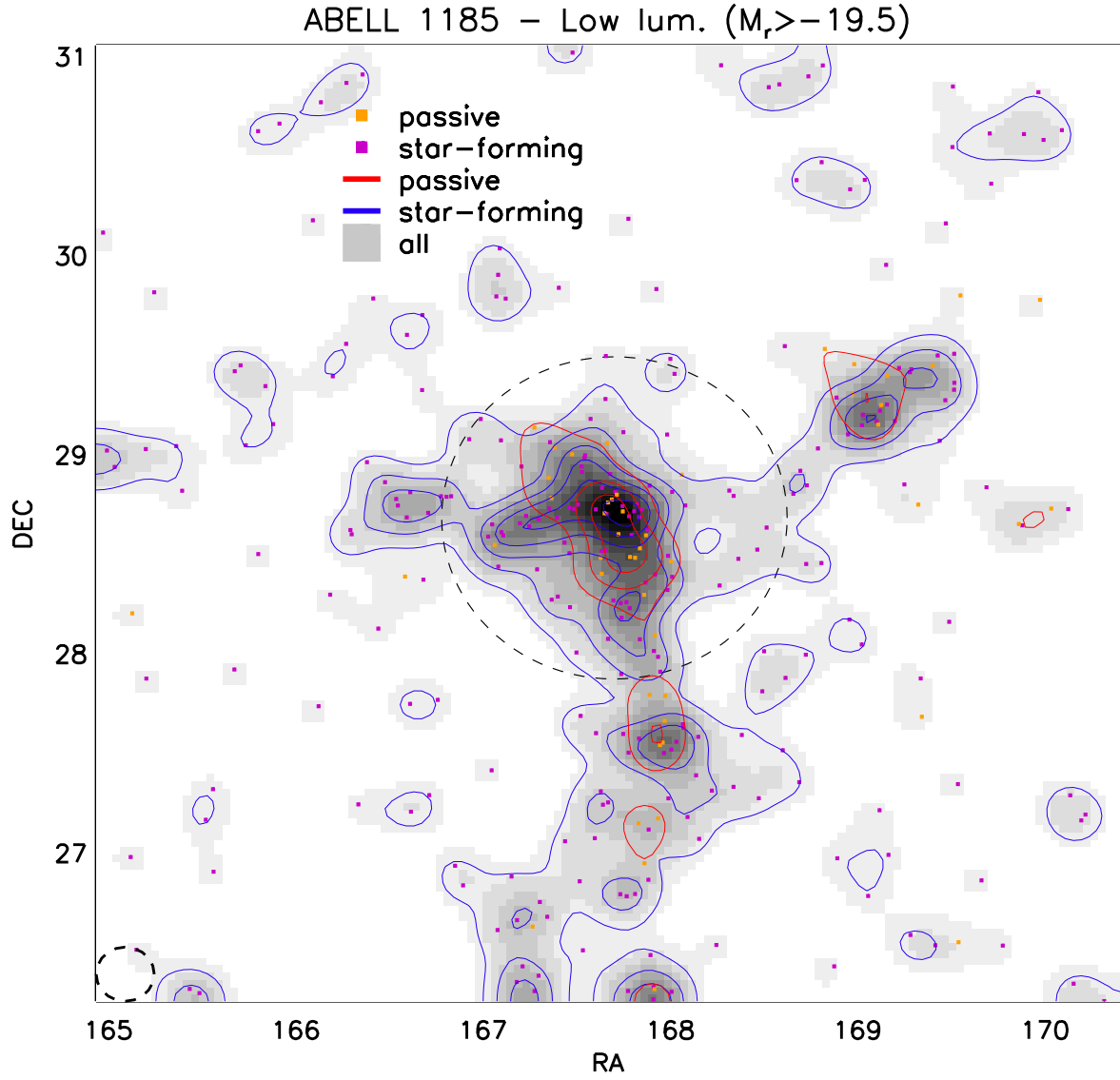


Fig. 11.— Sky projected density of low-luminosity  $-19.5 < M_r < -18$  galaxies around ABELL 1185. Color code, isodensity lines and the rest of elements of the figure are defined in the same way as figure 10.

of SDSS and other galaxy surveys from UV to FIR. We build a spectrophotometric catalogue for this cluster galaxy sample with a detailed photometry for each galaxy in order to be accurate for spectral template fitting.

- The clusters from the sample with X-ray detections or confident upper limits are consistent with the X-ray luminosity vs. cluster velocity dispersion  $L_X \propto \sigma_c^{4.4}$  trend found by Mahdavi & Geller (2001). The clusters with no X-ray fluxes in the literature can be reconciled with the  $L_X - \sigma_c$  trend assuming an upper limit in X-ray luminosity of  $10^{41}$  erg s<sup>-1</sup>, except for the case of WBL 205, a cluster with clear evidences of the presence of dynamical substructures.
- The galaxy density  $\Sigma_5$  distribution of virial regions are biased to higher densities with respect to the  $\Sigma_5$  distribution of the outskirts. The  $\Sigma_5$  distribution of massive clusters (virial regions and the outskirts) shows similar ranges than the low-mass clusters, but they have higher averages of  $\Sigma_5$  than the low-mass clusters and present a highest density tail which is missing in the low-mass clusters. The  $\Sigma_5$  distribution of virial regions of massive clusters is statistically distinguishable, up to a  $\sim 96$  % of probability, from the corresponding distribution for low-mass clusters. The overlapping of distributions of  $\Sigma_5$  between virial regions and their outskirts at highest densities suggests the presence of galaxy structures in the outskirts as massive as the cluster cores.
- The  $\Sigma_5 - r_P$  relation shows a more broad trend outside the virial region than the trend for the virial region, due to the presence of density peaks. Both the massive and low-mass clusters follow a similar trend inside the virial region, but the low-mass clusters avoid the highest density tail. This relation is well fitted by a King profile along the clustercentric radius, for both the massive and the low mass clusters.
- ABELL 1185 shows clear evidences of galaxy structures around the virial region. In

this cluster, low-luminosity star-forming galaxies are distributed along more spread structures than their giant counterparts, whereas low-luminosity passive galaxies avoid the low-density environment. Giant passive and star-forming galaxies share rather similar sky regions with passive galaxies exhibiting more cuspy distributions.

### Acknowledgements

J.D.H.F. thanks the Laboratoire d’Astrophysique de Marseille and L’Osservatorio Astronomico di Padova for hospitality during the stays to carry out part of this work. Special thanks are given to Veronique Buat, Denis Burgarella and Bianca M<sup>a</sup> Poggianti for their help and advice during the first stages of this work.

J.D.H.F. acknowledges financial support from the Spanish Ministerio de Ciencia e Innovación under the FPI grant BES-2005-7570. We also acknowledge funding by the Spanish PNAYA project ESTALLIDOS (grants AYA2007-67965-C03-02, AYA2010-21887-C04-01) and project CSD2006 00070 “1st Science with GTC” from the CONSOLIDER 2010 program of the Spanish MICINN.

This publication has made use of the following resources:

- the NASA/IPAC Extragalactic Database (NED) which is operated by the Jet Propulsion Laboratory, California Institute of Technology, under contract with the National Aeronautics and Space Administration.
- the Sloan Digital Sky Survey (SDSS) database. Funding for the Sloan Digital Sky Survey (SDSS) and SDSS-II has been provided by the Alfred P. Sloan Foundation, the Participating Institutions, the National Science Foundation, the U.S. Department of Energy, the National Aeronautics and Space Administration, the Japanese Monbukagakusho, and the Max Planck Society, and the Higher Education Funding



Council for England. The SDSS Web site is <http://www.sdss.org/>.

The SDSS is managed by the Astrophysical Research Consortium (ARC) for the Participating Institutions. The Participating Institutions are the American Museum of Natural History, Astrophysical Institute Potsdam, University of Basel, University of Cambridge, Case Western Reserve University, The University of Chicago, Drexel University, Fermilab, the Institute for Advanced Study, the Japan Participation Group, The Johns Hopkins University, the Joint Institute for Nuclear Astrophysics, the Kavli Institute for Particle Astrophysics and Cosmology, the Korean Scientist Group, the Chinese Academy of Sciences (LAMOST), Los Alamos National Laboratory, the Max-Planck-Institute for Astronomy (MPIA), the Max-Planck-Institute for Astrophysics (MPA), New Mexico State University, Ohio State University, University of Pittsburgh, University of Portsmouth, Princeton University, the United States Naval Observatory, and the University of Washington.

- the Galaxy Evolution Explorer (GALEX), which is a NASA mission managed by the Jet Propulsion Laboratory and launched in 2003 April. We gratefully acknowledge NASA's support for the construction, operation, and science analysis for the GALEX mission, developed in cooperation with the Centre National d'Etudes Spatiales of France and the Korean Ministry of Science and Technology.
- the Two Micron All Sky Survey (2MASS), which is a joint project of the University of Massachusetts and the Infrared Processing and Analysis Center at the California Institute of Technology, funded by the National Aeronautics and Space Administration and the National Science Foundation.
- the NASA/IPAC Infrared Science Archive, which is operated by the Jet Propulsion Laboratory, California Institute of Technology, under contract with the National Aeronautics and Space Administration.

## REFERENCES

- Abazajian, K., Adelman-McCarthy, J. K., Agüeros, M. A., et al. 2004, *AJ*, 128, 502
- Abazajian, K., Adelman-McCarthy, J. K., Agüeros, M. A., et al. 2003, *AJ*, 126, 2081
- Abell, G. O. 1958, *ApJS*, 3, 211
- Adelman-McCarthy, J. K., Agüeros, M. A., Allam, S. S., et al. 2008, *ApJS*, 175, 297
- Andreon, S. & Etti, S. 1999, *ApJ*, 516, 647
- Andreon, S., Quintana, H., Tajer, M., Galaz, G., & Surdej, J. 2006, *MNRAS*, 365, 915
- Baldwin, J. A., Phillips, M. M., & Terlevich, R. 1981, *PASP*, 93, 5
- Balogh, M., Eke, V., Miller, C., et al. 2004, *MNRAS*, 348, 1355
- Beers, T. C., Kriessler, J. R., Bird, C. M., & Huchra, J. P. 1995, *AJ*, 109, 874
- Bekki, K., Couch, W. J., & Shioya, Y. 2002, *ApJ*, 577, 651
- Bell, E. F., McIntosh, D. H., Katz, N., & Weinberg, M. D. 2003, *ApJS*, 149, 289
- Bertin, E. & Arnouts, S. 1996, *A&AS*, 117, 393
- Binggeli, B., Sandage, A., & Tammann, G. A. 1988, *ARA&A*, 26, 509
- Biviano, A., Katgert, P., Mazure, A., et al. 1997, *A&A*, 321, 84
- Blanton, M. R., Hogg, D. W., Bahcall, N. A., et al. 2003, *ApJ*, 594, 186
- Blanton, M. R., Schlegel, D. J., Strauss, M. A., et al. 2005, *AJ*, 129, 2562
- Boselli, A. & Gavazzi, G. 2006, *PASP*, 118, 517
- Cardelli, J. A., Clayton, G. C., & Mathis, J. S. 1989, *ApJ*, 345, 245

- Chilingarian, I. & Zolotukhin, I. 2011, ArXiv e-prints
- Colless, M., Dalton, G., Maddox, S., et al. 2001, MNRAS, 328, 1039
- Cowie, L. L. & Songaila, A. 1977, Nature, 266, 501
- Cox, A. N., ed. 2000, Allen’s Astrophysical Quantities (Springer-Verlag New York, Inc.)
- Cutri et al. 2001, Explanatory Supplement to the 2MASS Second Incremental Data Release,  
*<http://www.ipac.caltech.edu/2mass/releases/second/doc/explsup.html>*
- De Propris, R., Colless, M., Peacock, J. A., et al. 2004, MNRAS, 351, 125
- Ellingson, E., Lin, H., Yee, H. K. C., & Carlberg, R. G. 2001, ApJ, 547, 609
- Fairley, B. W., Jones, L. R., Wake, D. A., et al. 2002, MNRAS, 330, 755
- Finlator, K., Ivezić, Ž., Fan, X., et al. 2000, AJ, 120, 2615
- Finn, R. A., Zaritsky, D., McCarthy, Jr., D. W., et al. 2005, ApJ, 630, 206
- Fukugita, M., Ichikawa, T., Gunn, J. E., et al. 1996, AJ, 111, 1748
- Goto, T. 2005, MNRAS, 357, 937
- Gunn, J. E. & Gott, III, J. R. 1972, ApJ, 176, 1
- Haines, C. P., La Barbera, F., Mercurio, A., Merluzzi, P., & Busarello, G. 2006, ApJ, 647,  
L21
- Henry, J. P. & Arnaud, K. A. 1991, ApJ, 372, 410
- Hernández-Fernández, J. D. 2011, PhD thesis, Universidad de Granada
- Hernández-Fernández et al. 2011a, *Disentangling the role of environmental processes in galaxy clusters* (submitted)

- Hernández-Fernández et al. 2011b, *Galaxy projected distribution in a unbiased sample of nearby clusters* (submitted)
- Jarrett, T. H., Chester, T., Cutri, R., et al. 2000, AJ, 119, 2498
- Joint Iras Science, W. G. 1994, VizieR Online Data Catalog, 2125, 0
- Kaviraj, S., Kirkby, L. A., Silk, J., & Sarzi, M. 2007, MNRAS, 382, 960
- Kennicutt, Jr., R. C. 1998, ARA&A, 36, 189
- Kewley, L. J., Jansen, R. A., & Geller, M. J. 2005, PASP, 117, 227
- King, I. R. 1966, AJ, 71, 64
- King, I. R. 1972, ApJ, 174, L123
- Lupton, R., Gunn, J. E., Ivezić, Z., Knapp, G. R., & Kent, S. 2001, in Astronomical Society of the Pacific Conference Series, Vol. 238, Astronomical Data Analysis Software and Systems X, ed. F. R. Harnden Jr., F. A. Primini, & H. E. Payne, 269
- Lupton, R. 2005, Sloan to Johnson Photometric Transformations,  
<http://www.sdss.org/DR6/algorithms/sdssUBVRITransform.html#Rodgers2005>
- Madgwick, D. S., Hawkins, E., Lahav, O., et al. 2003, MNRAS, 344, 847
- Mahdavi, A., Böhringer, H., Geller, M. J., & Ramella, M. 2000, ApJ, 534, 114
- Mahdavi, A. & Geller, M. J. 2001, ApJ, 554, L129
- Margoniner, V. E., de Carvalho, R. R., Gal, R. R., & Djorgovski, S. G. 2001, ApJ, 548, L143
- Martin, D. C., Fanson, J., Schiminovich, D., et al. 2005, ApJ, 619, L1

- Martínez, H. J., Zandivarez, A., Domínguez, M., Merchán, M. E., & Lambas, D. G. 2002, MNRAS, 333, L31
- Mateo, M. L. 1998, ARA&A, 36, 435
- Mihos, J. C. 2004, Clusters of Galaxies: Probes of Cosmological Structure and Galaxy Evolution, 277
- Mobasher, B., Colless, M., Carter, D., et al. 2003, ApJ, 587, 605
- Moore, B., Katz, N., Lake, G., Dressler, A., & Oemler, A. 1996, Nature, 379, 613
- Moore, B., Lake, G., & Katz, N. 1998, ApJ, 495, 139
- Moore, B., Lake, G., Quinn, T., & Stadel, J. 1999, MNRAS, 304, 465
- Moshir, M., Copan, G., Conrow, T., et al. 1993, VizieR Online Data Catalog, 2156, 0
- Moustakas, J., Kennicutt, Jr., R. C., & Tremonti, C. A. 2006, ApJ, 642, 775
- Neugebauer, G., Habing, H. J., van Duinen, R., et al. 1984, ApJ, 278, L1
- Norberg, P., Baugh, C. M., Hawkins, E., et al. 2002, MNRAS, 332, 827
- Obrić, M., Ivezić, Ž., Best, P. N., et al. 2006, MNRAS, 370, 1677
- Poggianti, B. M., von der Linden, A., De Lucia, G., et al. 2006, ApJ, 642, 188
- Quilis, V., Moore, B., & Bower, R. 2000, Science, 288, 1617
- Rines, K., Geller, M. J., Kurtz, M. J., & Diaferio, A. 2003, AJ, 126, 2152
- Rines, K., Geller, M. J., Kurtz, M. J., & Diaferio, A. 2005, AJ, 130, 1482
- Sérsic, J. L. 1963, Boletín de la Asociación Argentina de Astronomía La Plata Argentina, 6, 41

Smail, I., Edge, A. C., Ellis, R. S., & Blandford, R. D. 1998, MNRAS, 293, 124

Springel, V., White, S. D. M., Jenkins, A., et al. 2005, Nature, 435, 629

Strateva, I., Ivezić, Ž., Knapp, G. R., et al. 2001, AJ, 122, 1861

Strauss, M. A., Weinberg, D. H., Lupton, R. H., et al. 2002, AJ, 124, 1810

Struble, M. F. & Rood, H. J. 1991, ApJS, 77, 363

Toniazzo, T. & Schindler, S. 2001, MNRAS, 325, 509

Wilman, D. J., Balogh, M. L., Bower, R. G., et al. 2005, MNRAS, 358, 71

Zabludoff, A. I. & Mulchaey, J. S. 1998, ApJ, 496, 39